Axial Offset Effects upon Optical Fiber Sensor and Splice Performance

by

Shiao-Chiu Lee

Thesis submitted to the Faculty of the
Virginia Polytechnic Institute and State University
in partial fulfillment of the requirements for the degree of
MASTER OF SCIENCE
in
Electrical Engineering

APPROVED:

Dr.R. O. Claus

Dr. C. W. Bostian

Dr. T. C. Poon

June,1985

Blacksburg, Virginia

AXIAL OFFSET EFFECTS UPON OPTICAL FIBER SENSOR AND SPLICE PERFORMANCE

by

Shiao-Chiu Lee

Committee Chairman: Richard O. Claus

Electrical Engineering

(ABSTRACT)

A kind of intensity modulated fiber sensor utilizing axial offset parameter is proposed. The theoretical analysis and experimental characteristics of this sensor are described.

All the theoretical results derived in this thesis are based on assuming a uniform power distribution in the fibers. An expression of coupling efficiency of central dipped parabolic graded index fibers due to axial offset is derived. The results show less sensitivity to axial offset for the central dipped fibers than for the parabolic profile fibers without a dip. Expressions of coupling efficiency of graded index fibers due to axial offset for several different values of α are also derived. The results show that sensitivity increases as the value of α decreases. A general expression of coupling efficiency which is valid for small values of

axial offset is derived. This expression exhibits a linear relationship between coupling efficiency and small axial offset.

Coupling efficiencies versus fiber end separation and axial offset of step index fibers have been measured. The measurements show that coupling efficiency is much more sensitive to axial offset than end separation. A simple construction of the axial offset fiber sensor is described. An approximate linear relationship between the output power and the mechanical loading has been obtained for this sensor. Several ways of increasing the sensitivity of this sensor are discussed.

ACKNOWLEDGEMENTS

I wish to thank my advisor, Dr. Richard O. Claus, for his time, patience and encouragement. I would also like to thank Dr. Charles W. Bostian and Dr. Ting-Chung Poon for their comments and suggestions.

I wish to thank the Department of Electrical Engineering and NASA for providing financial support.

I am also grateful to Kim Bennett and Michael Barsky for their help and suggestions. Finally, I want to thank my family for their love and support.

TABLE OF CONTENTS

LIST OF FIGURES

CHAPTER I

INTRODUCTION

Fiber optic technology has been developing rapidly since Charles Kao and George Hockham proposed the use of optical fiber waveguides for information transmission in 1966 [1]. The importance of optical fiber waveguides in communications has encouraged improvements in light sources, optical fibers and photodetectors. Capitalizing on the availability of optical components, there also has been significant progress during the past few years toward the development of a new class of sensors employing fiber optics. These sensors respond to pressure, temperature, acoustic fields, electric fields, magnetic fields, displacement, rotation rates, acceleration, chemical concentration gradients and many other physical parameters.

The advantages of fiber sensors over conventional sensors are freedom from electromagnetic interference, chemical inertness, spark free operation, low weight, and small volume. Fiber sensors are particularly applicable to the power, process control and avionic industries, and for robotic systems. Furthermore, fiber sensors are particularly attractive

for the nondestructive measurement of stress in composite materials. The advantages of fiber sensors in such an application are [2] :

1. The geometry of an optical fiber would lay well with the fibers in a fiber-laminate. Any sensor within a composite that existed as a discrete block would provide a discontinuity in the material, concentrating stress, and inviting failure. Optical fiber, on the other hand, could lay within a fiber-laminate composite without seriously compromising its structural integrity.

2. Optical fiber imbedded in the composite would result in few if any dimensional changes of the composite. Conversely, external sensors would cause gross dimensional changes in the composite that would not be tolerable in many applications.

3. Optical fiber is all-dielectric. Laminating it into a dielectric fiber-laminate composite would maintain its all-dielectric nature. This is important where composites may be used in high EM environments.

Fiber optic sensors may conveniently be divided into two main types. The first type, the intrinsic sensor, is constructed using the fiber as the sensing element, and arranging for the physical parameter to be monitored to modify the transmission properties. Examples of intrinsic sensors are those based on microbending and modulation of the evanescent field around the fiber core [3]. The second type, the extrinsic sensor, uses the optical fiber purely as a means of transmitting light to and from the sensor. An example is the moving grating fiber optic sensor [3]. In both types of sensors the measurand is used to modulate the light by intensity, phase, polarization, wavelength or by frequency. Among these modulation schemes, the two simpler and more commonly used modulations are intensity modulation and phase modulation.

1.1 PHASE MODULATED SENSORS

Single mode fiber Mach-Zehnder interferometer sensors are typical phase modulated sensors. The geometry of the sensor is shown in Figure 1.1. If the optical path lengths of the two arms are equal, the light from the two fibers interferes to form a series of bright and dark fringes. A change in the relative phase of the light from one fiber with

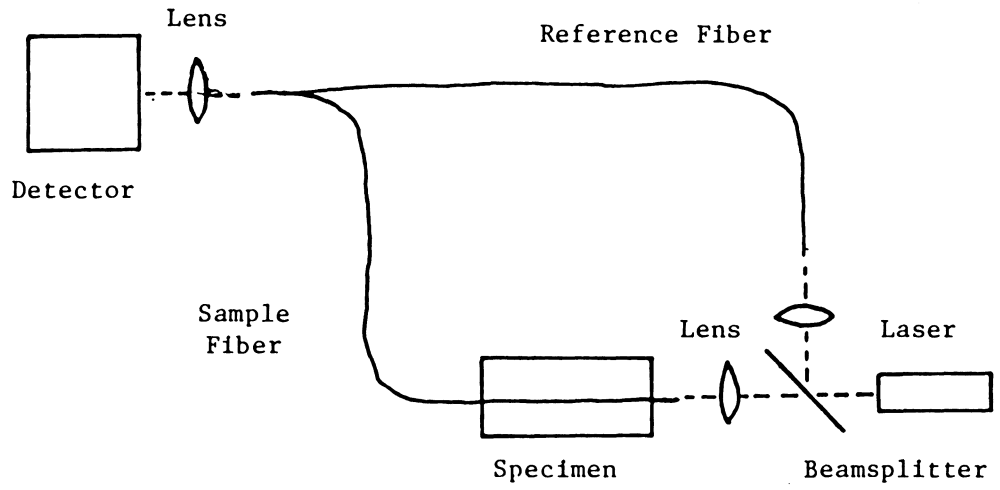

Figure 1.1. Mach-Zehnder interferometer sensor geometry [4].

respect to the other is observed as a displacement of the fringe pattern, a phase change of 2π radians causing a displacement of one fringe. Thus, if one fiber is subject to a different pressure than the other, this difference appears as a displacement of the fringes and can be measured by this displacement.

To determine the sensitivity of the fiber, consider a fiber of length L, core diameter D, and core index of refraction n. If the laser light has a single mode propagation constant K inside the fiber, then the phase of the light wave after going through this fiber section is $\phi=KL$. Straining the fiber causes the phase at the output to shift by

$$\Delta\phi = K\Delta L + L\Delta K \qquad (1.1)$$

The first term represents the effect of the physical change of length due to the pressure. The second term, the change in ϕ due to a change in K, can come about from two effects : the strain-optic effect whereby the strain changes the refractive index of the fiber, and a waveguide mode dispersion effect due to a change in fiber diameter produced by the pressure :

$$L\Delta K = L \frac{\partial K}{\partial n}\Delta n + L \frac{\partial K}{\partial D}\Delta D \qquad (1.2)$$

For an ITT-110 single mode optical fiber the phase shift per unit pressure per unit length is approximately 4.09×10^{-5} rad/Pa-m [4].

The sensitivity of this type of sensor can be increased by using a suitable fiber coating [3].

1.2 INTENSITY MODULATED SENSORS

The intensity-modulation sensor employs relatively more simple optics and circuitry than other types of sensors. Its basic configuration is sketched in block diagram form in Figure 1.2. The output light wave from an optical source of constant intensity I_{in} is injected into the sensing element. This element, acted on by an external force field (baseband signal), represented in the figure as an incident sinusoidally-varying quantity, alters the intensity of the light transmitted through the sensor. The modulation envelope of the output intensity, I_{out} , matches that of the input force field (signal). In turn, the time varying output optical intensity, incident on the photodetector, similarly modulates the output voltage, e_{out}.

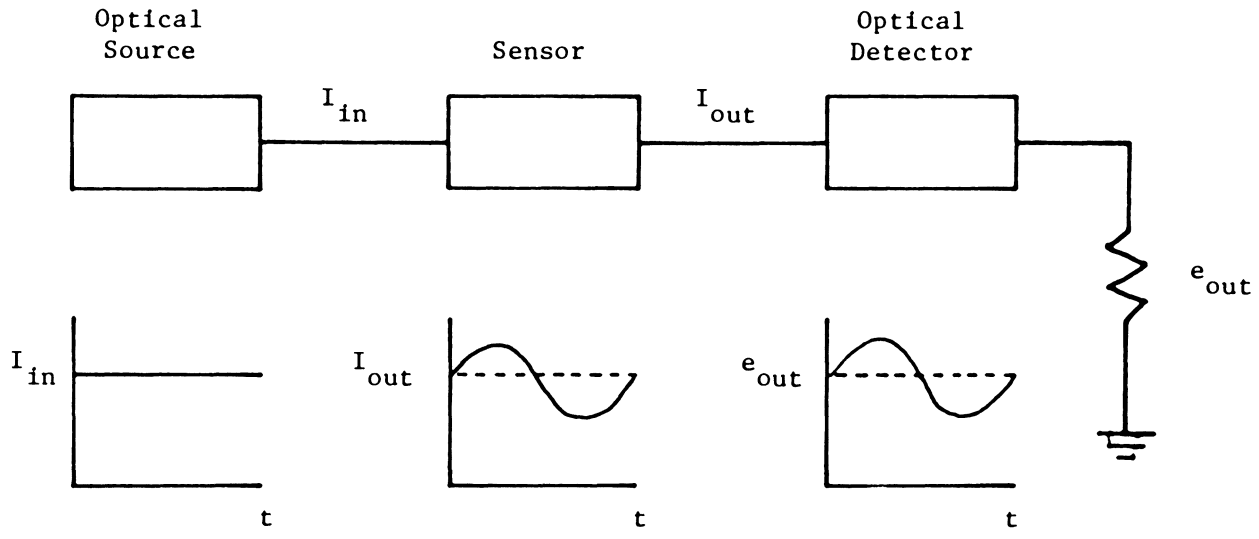

Figure 1.2. A generalized intensity-type fiber optic sensing system.

Microbend fiber optic sensors are very commonly used intensity-type sensors [3,5]. These sensors are based on microbend-induced ejection of light from the core of a fiber into the cladding. Referring to Figure 1.3, the transduction element in this type of sensor consists of a deforming device such as a pair of toothed plates that introduce small bends in a fiber. As shown in the figure, the distance L between adjacent teeth defines the spatial frequency of the deformer. Based on a ray description, rays propagating in a straight section of the fiber core at an angle less than the critical angle will have their angle of incidence to the core-cladding interface increased by the bends and thus be partially transmitted into the cladding. Increasing the amount of deformation increases the amount of light coupled out of the fiber core and into the cladding. If the deformation is caused by the signal being detected (pressure, sound, etc.), the fluctuation in intensity of either the core or cladding light will be directly proportional to the signal for small deformations. Thus by monitoring either the core or cladding light, the signal can be detected.

Since high order modes rather than low order modes are converted to radiating modes by microbending, the sensitivity of microbend fiber optic sensors can be increased by prefer-

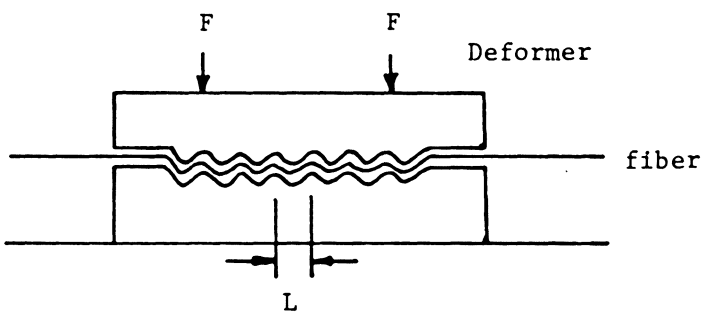

Figure 1.3. A microbend intensity-type fiber optic sensor [3].

ential propagation of leaky or lossy modes. One way of achieving this is by varying the angle of incidence at the fiber endface. Another way of increasing the sensitivity is by using parabolic graded-index fibers with a central dip [6]. This refractive index profile enhances guidance of high order skew modes over low order meridonal modes. It is frequently encountered in fibers fabricated with the modified chemical vapor deposition (MCVD) process.

1.3 COUPLING SENSORS

The great sensitivity of optical fiber to environment influence has been considered as a kind of disadvantage in the application as an information transmission medium. A considerable amount of research has been directed towards the minimization of the fiber's sensitivity. On the other hand, this sensitivity is used and maximized in the applications as fiber optic sensors.

Following the fundamental research leading to the availability of critical components, such as low loss fiber and long-life sources, attention was concentrated on reducing sensitivity of coupling loss between fibers.

Splice losses or coupling losses between fibers can be divided into two categories. The first category of losses is related to the technique used to join fibers and is caused by extrinsic parameters such as transverse offset between the fiber cores, end separation, axial tilt and fiber end quality. The second category of losses is related to the properties of the fibers joined and is referred to as intrinsic splice loss. Intrinsic parameters include variations in fiber diameter (both core and cladding), index profile (α and Δ mismatch), and ellipticity and concentricity of the fiber cores.

Splice loss is significantly more sensitive to transverse offset (axial offset) and axial tilt than it is to longitudinal offset. Fiber end quality has a minimum effect on splice loss if proper fracturing or grinding and polishing end-preparation techniques are used in conjunction with an index-matching material. A matching material with a refractive index approximately the same as that of the core is used to reduce the Fresnel reflection loss caused by the glass-air interfaces between the coupled fibers of a joint.

The mismatch of intrinsic parameters can also significantly affect the coupling loss. Splice loss is most sensi-

tive to a mismatch of Δ or core radius, where Δ is the fractional difference between the refractive indices of the core and the cladding. Sensitivity of splice loss to α mismatch is substantially less than that for Δ or core-radius mismatch.

1.4 REPORT OVERVIEW

Among all these parameters, coupling loss is most sensitive to transverse offset. This report describes a kind of intensity modulated fiber sensor utilizing transverse offset parameter. The theoretical analysis and experimental characteristics of this sensor are described in the following chapters.

Chapter 2 begins with a discription of optical fiber structure. Then both ray theory and EM wave theory are used to describe the light propagation mechanism. This chapter ends with discussion of power and rise time budgets. Chapter 3 provides a general idea of fiber-to-fiber coupling theory which includes coupling efficiency due to intrinsic and extrinsic parameters of both step index and parabolic graded index fibers. Chapter 4 gives derivations of coupling efficiency of graded index fibers with different refractive index

profiles due to axial offset. This chapter ends with a short discussion of results from several papers. Experimental results of coupling efficiency due to longitudinal separation and axial offset are shown in chapter 5. The construction of an axial offset fiber optic sensor is described in this chapter. Finally, the last chapter concludes this report.

CHAPTER II

THEORY OF LIGHT PROPAGATION IN OPTICAL FIBERS

The theoretical study of the propagation characteristics of light in an optical fiber may be carried out using two different approaches, namely ray theory and electromagnetic wave theory. Before these propagation theories are discussed, it is necessary to introduce the structure of the three commonly used fibers.

2.1 CLASSIFICATION

The physical structure of fiber waveguides consists of three concentric layers : the core, the cladding, and the jacket. The core and the cladding are mainly silicon dioxide, while the jacket is usually an organic polymer. The index of refraction of the core is larger than that of the cladding.This difference in refractive index causes total internal reflection. The jacket's main function is to protect the fiber from abrasion without degrading optical performance.

Optical fibers may be classified in terms of the refractive index profile of the core and by whether one mode or many modes are propagating in the guide. If the core has a uniform refractive index n_1 it is called a step-index fiber. If the core has a nonuniform refractive index that gradually decreases from the center toward the core-cladding interface, the fiber is called a graded-index fiber. The cladding surrounding the core has a uniform refractive index $n_2 = n_1(1-\Delta)$ that is slightly lower than the refractive index of the core region. The most common graded-index fiber has a core profile which is parabolic with respect to radius. Figure 2.1 shows refractive indices for commonly used fibers. Typical multimode fibers have 50μm core diameter and 125μm cladding diameter. Typical single mode fiber dimensions are 5-12μm core and 100μm cladding diameters.

2.2 RAY THEORY

In accordance with the ray theory of light propagation, a light beam incident from below at an angle θ_1 with the interface surface between two transparent media behaves as shown in Figure 2.2. When θ_1 is large, part of the incident beam is transmitted into the upper medium and part is reflected. Their relative intensities depend upon the

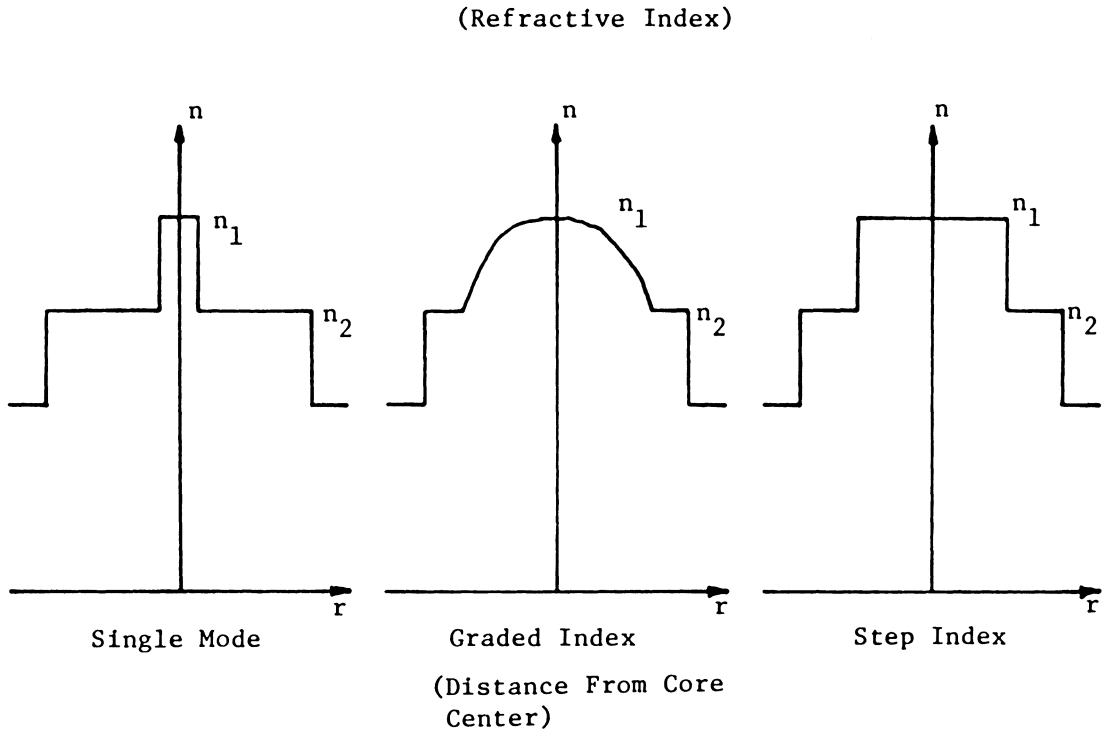

Figure 2.1. Refractive indices of commonly used fibers.

refractive indices of the two media. The refractive index of medium 1 is designated as n_1 and that of medium 2 as n_2 as shown in Figure 2.2. The direction of the beam transmitted into medium 2 can be determined by applying Snell's law,

$$n_1 \cos\theta_1 = n_2 \cos\theta_2 \tag{2.1}$$

As the angle θ_1 is decreased the refracted beam entering medium 2 bends toward the interface until finally the angle θ_2 reaches zero. At the same time the intensity of the light entering medium 2 approaches zero. Thus the intensity of the reflected beam approaches that of the incident beam. The value of θ_1 corresponding to the limiting value of $\theta_2=0$ is defined as the critical angle $\theta c'$. It is given by

$$\theta c' = \cos^{-1} \frac{n_2}{n_1} \tag{2.2}$$

For all values of angle θ_1 equal to or less than the critical angle $\theta c'$, the incident ray will be totally reflected and energy will not be transmitted into medium 2. It should be emphasized that this phenomenon of total internal reflection at an interface occurs only when the refractive index n_1 is greater than the refractive index n_2. This phenomenon is the basis of operation of optical fibers.

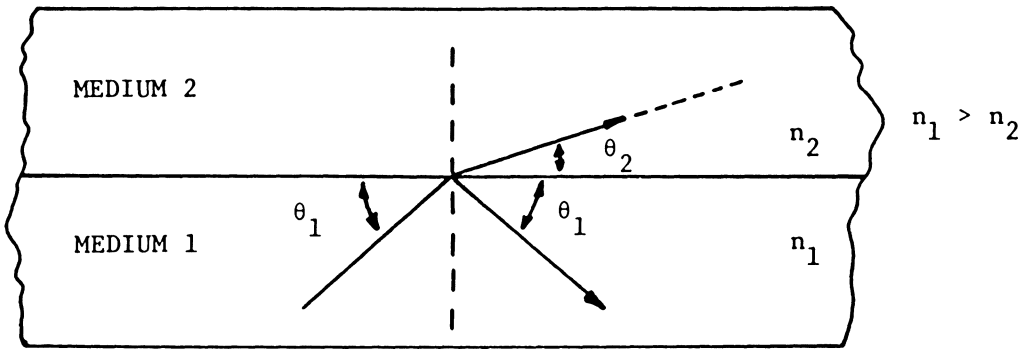

Figure 2.2. Reflection and refraction at the interface when a lightwave travels from a higher to a lower refractive index medium.

The refractive index of the cladding is held slightly less than that of the core and thus it is convenient to introduce a quantity Δ , the fractional difference between the two refractive indices, defined by the equation :

$$\Delta = \frac{n_1 - n_2}{n_1} \qquad (2.3)$$

As previously stated, rays propagating in the core at angles equal to or less than $\theta c'$ will be trapped in the core while rays that propagate at angles θ_1 greater than $\theta c'$ will be partially transmitted into the cladding each time they encounter the core-cladding interface. These latter rays rapidly decrease in intensity as they travel through the core and thus do not propagate over long distances in fibers.

Meridonal rays (rays that travel in a plane containing the central axis of the core) for the step-index fiber and for the graded-index fiber are shown in Figure 2.3 a and b respectively. The meridonal rays for the graded-index fiber propagate along curved lines, rather than traveling along straight lines. They are continuously being bent back and forth. This is because the index varies continuously from the center of the core out to the core-cladding interface.

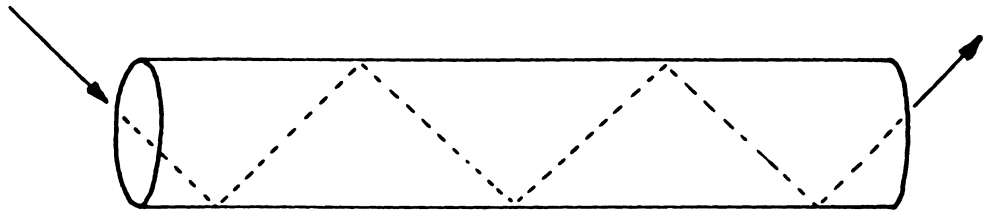

(a) Step-index fiber

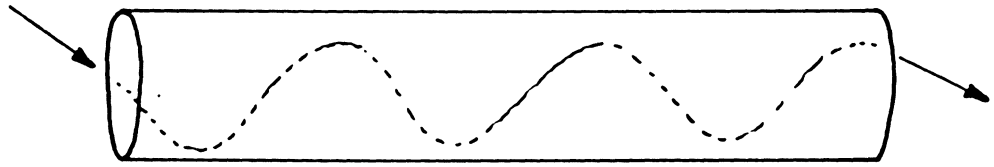

(b) Graded-index fiber

Figure 2.3. Meridonal ray geometry.

The numerical aperture (NA) of an optical fiber is defined as the sine of the half-angle of the cone of light that is incident from air on the input end of an optical fiber, such that all the rays having a direction that lies within the core will be trapped within the core once they enter the fiber as shown in Figure 2.4. Thus at the core-air transverse interface end surface, where the refractive index of air, n_o, is equal to unity, there is a critical angle $\theta c'$, such that all the light contained within the core of half angle θc, will be trapped within the fiber. Applying Snell's law,

$$\sin\theta c' = \frac{\sin\theta c}{n_1} \tag{2.4}$$

After some algebraic manipulation, numerical aperture may be written as,

$$N A = \sin\theta c = (n_1^2 - n_2^2)^{\frac{1}{2}} \tag{2.5}$$

If $\Delta^2 << 2\Delta$, which is usually the case for optical fiber, then

$$N A = n_1(2\Delta)^{\frac{1}{2}} = [2n_1(n_1-n_2)]^{\frac{1}{2}} \tag{2.6}$$

Eq.(2.6) states that the amount of light that will remain trapped and propagate in the core is directly proportional

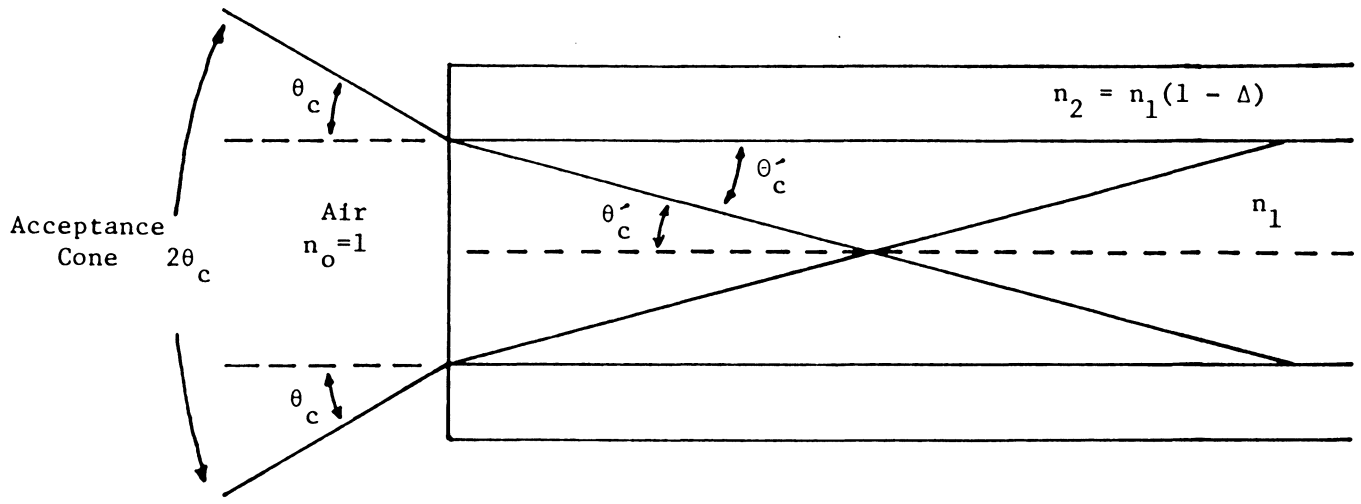

Figure 2.4. The acceptance cone for a step-index optical fiber.

to the square root of the product of the core refractive index and the core-cladding refractive index difference.

2.3 ELECTROMAGNETIC WAVE THEORY

The ray theory is an approximate representation of light propagation in confined media. It applies only at wavelengths that are small in comparison to the dimensions of the cross section of the waveguide. Since optical fibers are cylindrical waveguides, " small " is in comparison to the radius of the core. For helium-neon light the wavelength is 0.63 μm and the ray theory applies well to fibers with a core radius greater than 25 μm. For guides with a core radius of 2 μm, the ray theory is a poor approximation since in this case the wavelength is only about one third of the core radius. Therefore, electromagnetic wave theory is used to obtain a good representation or description of light propagation [2].

2.3.1 STEP-INDEX FIBER

Working with Maxwell's equations on fiber waveguides, one may derive the following wave equations for the longi-

tudinal electric (E) and magnetic (H) field components in cylindrical coordinates [7]:

$$\frac{\partial^2 E_z}{\partial r^2} + \frac{1}{r}\frac{\partial E_z}{\partial r} + \frac{1}{r^2}\frac{\partial^2 E_z}{\partial \phi^2} + q^2 E_z = 0 \qquad (2.7)$$

$$\frac{\partial^2 H_z}{\partial r^2} + \frac{1}{r}\frac{\partial H_z}{\partial r} + \frac{1}{r^2}\frac{\partial^2 H_z}{\partial \phi^2} + q^2 H_z = 0 \qquad (2.8)$$

where $q^2 = \omega^2 \varepsilon \mu - \beta^2 = k^2 - \beta^2$ and β is the z component of the propagation vector. The solutions of equations (2.7) and (2.8) are of the same form. Solutions to the first equation will be developed here.

First it is assumed that the solution to (2.7) can be written in terms of independent functions of r and ϕ. Let

$$E_z(\phi, r) = A\Phi(\phi)\, F(r) \qquad (2.9)$$

where $\Phi(\phi) = e^{j\nu\phi}$ and ν is a positive or negative integer.

Substituting (2.9) into (2.7) and applying separation of variables and elementary calculus, the following equation is obtained :

$$\frac{d^2F(r)}{dr^2} + \frac{1}{r}\frac{dF(r)}{dr} + (q^2 - \frac{\nu^2}{r^2})F(r) = 0 \qquad (2.10)$$

Equation (2.10) must now be solved for the regions inside and outside the core. For the inside region the solutions for the guided modes must remain finite as $r \to 0$, whereas on the outside the solutions must decay to zero as $r \to \infty$ Thus for $r<a$, (where a is the radius of the core), the solutions are Bessel functions of the first kind of order ν. For these functions we use the common designation $J\nu(ur)$. Here $u^2 = k_1^2 - \beta^2$ with $k_1 = 2\pi n_1/\lambda$. The expressions for E_z inside the core is

$$E_z = AJ\nu(ur)e^{j\nu\phi} \qquad (2.11)$$

where A is an arbitrary constant.

Outside of the core the solutions to Eq.(2.10) are given by modified Bessel functions of the second kind $K\nu(wr)$, where $w^2 = \beta^2 - k_2^2$ with $k_2 = 2\pi n_2/\lambda$ [7]. The expression for E_z outside the core is, therefore,

$$E_z = BK\nu(wr)e^{j\nu\phi} \qquad (2.12)$$

where B is an arbitrary constant.

From the definition of the modified Bessel function, it is seen that $K_\nu(wr) \to e^{-wr}$ as $wr \to \infty$. Since $K_\nu(wr)$ must go to zero as $r \to \infty$, it follows that $w>0$. This in turn implies that $\beta \geq k_2$, which represents a cutoff condition. The cutoff condition is the situation at which a mode is no longer bound to the core region. A second condition on β can be deduced from the behavior of $J_\nu(ur)$. Inside the core the parameter u must be real for F(r) to be real, from which it follows that $k_1 \geq \beta$. The permissible range of β for bound solutions is, therefore,

$$n_2 k_o \leq \beta \leq n_1 k_o \tag{2.13}$$

where $k_o = 2\pi/\lambda$ is the free-space propagation constant.

2.3.2 GRADED-INDEX FIBER

For a guide with radial variation of index n(r), Eq. (2.10) may be rewritten

$$\frac{d^2F(r)}{dr^2} + \frac{1}{r}\frac{dF(r)}{dr} + \left[k^2(r) - \beta^2 - \frac{\nu^2}{r^2}\right] F(r) = 0 \tag{2.14}$$

where $k(r) = 2\pi n(r)/\lambda$.

Application of the WKBJ technique [7] assumes a solution for (2.14) of the form

$$F(r) = e^{jk_o S(r)} \tag{2.15}$$

Substituting (2.15) into (2.14) and after some simplifications yields

$$-\left(\frac{dS_o}{dr}\right)^2 k_o^2 + \left[k^2(r) - \beta^2 - \frac{\nu^2}{r^2}\right] = 0 \tag{2.16}$$

where $S_o(r)$ is the first term of the power-series approximation of $S(r)$:

$$S(r) = S_o(r) + \frac{1}{k_o} S_1(r) + \frac{1}{k_o^2} S_2(r) + \ldots\ldots \tag{2.17}$$

To obtain information about the modes in a graded-index fiber, Eq. (2.16) should be solved for $S_o(r)$:

$$S_o(r) = \pm \frac{1}{k_o} \int_{r_1}^{r_2} \left[k^2(r) - \beta^2 - \frac{\nu^2}{r^2}\right]^{1/2} dr \tag{2.18}$$

A knowledge of $S_o(r)$ will yield, as a zero-order WKBJ approximation, that $F(r)$ from Eq. (2.15) is

$$F(r) = e^{jk_o S_o(r)} \tag{2.19}$$

From Eq. (2.19), for a propagating mode to exist, $S_o(r)$ must be real. This requires

$$k^2(r) - \beta^2 - \frac{\nu^2}{r^2} > 0 \tag{2.20}$$

To obtain a physical interpretation of bound modes, Eq. (2.20) is analyzed graphically. Figure 2.5a illustrates $k^2(r)$ and ν^2/r^2 as a function of the radius r. The curve in Figure 2.5b shows $k^2(r) - \nu^2/r^2$ as a function of r. For a fixed value of β there exists two values of r (r_1 and r_2) which

$$k^2(r) - \frac{\nu^2}{r^2} - \beta^2 = 0 \tag{2.21}$$

It is between these two radii that the ray associated with the assumed plane wave solution is constrained to move. Outside of these two values of r, called the turning points, $S_o(r)$ becomes imaginary, leading to decaying fields.

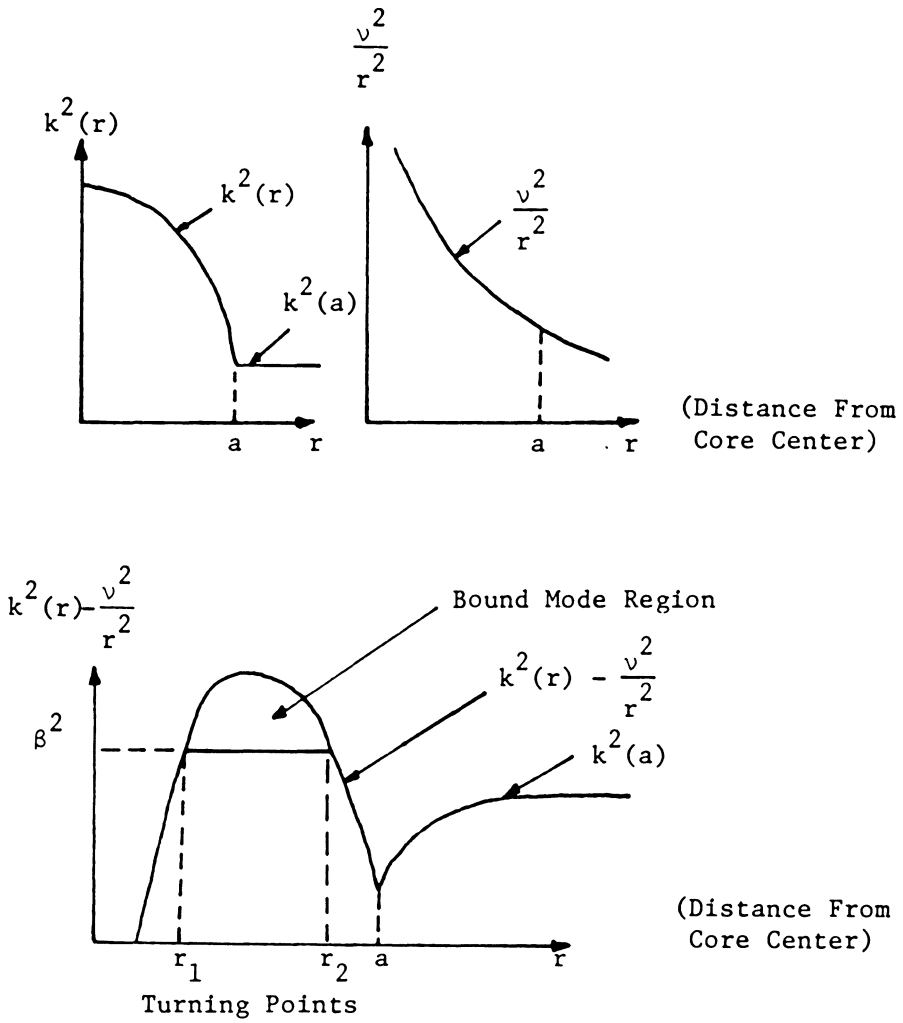

Figure 2.5. Wave-number diagram for graded-index fiber [7].

2.4 PROPERTIES OF FIBER WAVEGUIDES

2.4.1 ATTENUATION

Attenuation of a light signal as it propagates along a fiber is an important consideration in the design of an optical fiber system. The basic attenuation mechanisms are absorption, Rayleigh scattering, and radiative losses of optical energy.

1. Absorption

Absorption is defined as the conversion of light energy to heat. Light absorption occurs at wavelength λ, for which the relation

$$\lambda = \frac{hC}{E_2 - E_1} \tag{2.22}$$

holds. In this formula E_1 and E_2 are the initial and final energy states of either an electronic or a vibrational level scheme, the electron or the molecule absorb a photon of wavelength λ and make a transition from E_1 to E_2; h is Planck's constant and c the velocity of light in vacuum.

Absorptions may be divided into two categories, intrinsic and impurity absorptions. Intrinsic absorption is caused by the basic constituent atoms of the fiber material. This material (fused silica) has very strong electronic absorption bands in the ultraviolet wavelength region and vibrational absorption bands in the infrared wavelength region. It is very difficult, however, to produce fused silica of perfect purity. Additional absorptions occur if the silica is contaminated with ions of transition metals or with water. The transition metals copper, iron, nickel, chromium, and manganese usually occur in the host material as ions that have electronic absorption lines in or near the visible part of the spectrum.

2. Rayleigh Scattering

Rayleigh scattering arises from the variations in refractive index which occur within the glass over distances that are small compared with the wavelength of the scattered light. Such index variations are caused by local fluctuations in composition and density within the glass and are very dependent on the basic glass and its method of preparation. There is , however, a lower limit to the Rayleigh scatter which also dominates the theore-

tical limit for the reduction of loss in the material. Rayleigh scattering loss exhibits a characteristic variation as λ^{-4}.

3. Radiative Losses

Radiative losses occur whenever an optical fiber is bent. Fibers can be subject to two types of bends : (a) bends having radii that are large compared to the fiber diameter, for example, such as occur when a fiber cable turns a corner, and (b) microbends, which are random microscopic bends of the fiber axis that can arise when the fibers are incorporated into cables. Microbending is a characteristic of fibers which is employed in fiber optic sensors as a transduction mechanism.

2.4.2 DISPERSION

An optical signal becomes increasingly distorted as it travels along a fiber. This distortion is a consequence of intramodal and intermodal dispersion.

1. Intramodal dispersion

Intramodal dispersion has two causes : the nonzero spectral width of the optical signal generator and the variation in the propagation constant of light in the fiber as a function of wavelength. Part of this variation comes from the change of the index of refractive with wavelength and is called material dispersion. Another part arises because the propagation constant depends on the ratio of core radius to the wavelength of the light, and this part is called waveguide dispersion.

Material dispersion is given by [7,11]

$$\tau_{mat} = -\frac{L}{C} \lambda \frac{d^2 n}{d\lambda^2} \sigma_\lambda \qquad (2.23)$$

where σ_λ is the spectral width of the source, and L is the fiber length.

Waveguide dispersion is small over most of spectral range of interest and is important only in single mode fibers. In the absence of material dispersion, waveguide dispersion, τ_w, is given approximated by [8]

$$\tau_w = -\frac{L\sigma_\lambda}{2\pi C} V^2 \frac{\partial^2 \beta}{\partial V^2} \qquad (2.24)$$

where $v = 2\pi a(n_1 - n_2)^{\frac{1}{2}} / \lambda$ and β is the propagation constant of the fundamental mode of the fiber.

2. Intermodal Dispersion

The rays which travel parallel to the fiber axis arrive sooner than those making many reflections. Each pulse of light launched into the fiber core is made up of many rays, and the difference in arrival times broadens the pulse. This is called intermodal dispersion. This type of dispersion is eliminated in single mode fiber. The intermodal dispersion is minimum in approximately parabolic graded index fibers. Intermodal dispersion is given by [9]

$$\tau_{intermodal} = \frac{LN_1\Delta}{2C} \frac{\alpha}{\alpha + 1} \left(\frac{\alpha + 2}{3\alpha + 2}\right)^{1/2} x$$

$$\left[C_1^2 + \frac{4C_1C_2(\alpha + 1)\Delta}{2\alpha + 1} + \frac{16\Delta^2C_2^2(\alpha + 1)^2}{(5\alpha+2)(3\alpha+2)}\right]^{1/2} \qquad (2.25)$$

where

$$C_1 = \frac{\alpha - 2 - \varepsilon}{\alpha + 2}$$

$$C_2 = \frac{3\alpha - 2 - 2\varepsilon}{2(\alpha + 2)}$$

$$\varepsilon = \frac{2n_1 k}{N_1 \Delta} \frac{\partial \Delta}{\partial k}$$

$$N_1 = n_1 + k \frac{\partial n_1}{\partial k}$$

and α is a parameter that describes the shape of the refractive index profile. The root-mean square pulse broadening in a fiber can be obtained from [10]

$$\tau = (\tau^2_{\text{intermodal}} + \tau^2_{\text{intramodal}})^{1/2} \qquad (2.26)$$

2.5 TELEMETRY SYSTEM BUDGETS

A fiber optic sensor is a transducer which provides the transform that enables an on site measurement of a physical parameter to be represented in a form that can be directly processed. Most applications will require that the signal from a sensor be telemetered to a location other than the point of its generation. This section will be devoted to the analysis of fiber optic telemetry or communication system budgets.

2.5.1 POWER BUDGET

For a point-to-point link, the optical power received at the photodetector depends on the amount of light coupled into the fiber and the losses occuring in the fiber and at the connectors and splices. The link loss budget is derived from the sequential loss contributions of each element in the link.

A link power margin is normally provided in the analysis to allow for component aging, temperature fluctuations, and losses arising from components that might be added at future dates. A link margin of 6 dB is generally used for systems that are not expected to have additional components incorporated into the link in the future.

The link loss budget considers the total optical power loss P_T that is allowed between the light source and the photodector, and allocates this loss to cable attenuation, coupling loss, connector loss, splice loss and system margin.Thus if P_S is the average power lauched into fiber, and if P_R is the receiver sensitivity, then

$$P_T = P_S - P_R = 2L_c + 5L_s + \alpha_f L + \text{system margin} \quad (2.27)$$

Here L_c is the connector loss, L_s is the splice loss, and α_f is the fiber attenuation (dB/km).The assumed cable has length L, two connectors and five splices. Typical connector and splice losses are 1 dB and 0.5 dB respectively.

2.5.2 RISE TIME BUDGET

A rise time budget analysis is a convenient method for determining the dispersion limitation of an optical fiber link. The total link risetime is the root mean square of the transmitter, fiber cable and receiver rise times. However, these components themselves may have serial elements, each with individual rise times. For example, the transmitter may have an electronic rise time and a fiber optic pigtail and coupler rise time [3].The cable may have splices or repeaters. All the rise times of these are combined on the same RMS basis [11].

The rise times of transmitters and receivers are generally know to the link designer. The transmitter rise time is attributable primarily to the light sources and its drive circutry. The receiver rise time results from the

photodetector response and the 3-dB electric bandwidth of the receiver front end. If B_{rx} is the 3-dB electric bandwidth of the receiver in MHz, then the receiver front end rise time in ns is given by the standard empirical formula [11]

$$t_{rx} = \frac{350}{B_{rx}} \tag{2.28}$$

An empirical expression for the fiber risetime due to modal dispersion is [11]

$$t_{mod} = \frac{440L^{P}}{B_{o}} \tag{2.29}$$

where B_o is the bandwidth of a 1-km length of cable. A value of P=0.5 indicates that a steady state modal equilibrium has been reached, where P=1 indicates little mode mixing. Based on field experience, a reasonable estimate is P=0.7 [11].

Material dispersion effects can be neglected for laser sources, and for light emitting diodes (LEDs) at long wavelengths. For LEDs at short wavelengths, material dispersion adds about 0.07ns/(nm-km) to the rise time [11].

The total rise time for the link cannot exceed the maximum allowable rise time for the link. In digital systems,

the allowable rise time is limited by the requirement to prevent the bit error rate due to intersymbol interterence from exceeding a prescribed value. For example, in the nonreturn-to-zero (NRZ) method of signal representation (code), the rise time of the system, t_r must be less than 0.7 times the bit interval, expressed as the reciprocal of the bit rate. For return-to-zero (RZ) coding the factor is 0.5.

The greater the power loss, the cheaper the components. At the same time, the longer the rise time, the cheaper the components. Therefore, judicious maximal use of available rise time and minimal use of power are very important factors for reducing the cost of a fiber optic telemetry system.

CHAPTER III

GENERAL DESCRIPTION OF FIBER-TO-FIBER COUPLING THEORY

3.1 INTRODUCTION

Optical power injection into a fiber is one of the most important problems in fiber optic systems. A large amount of power is lost in the coupling region between source and fiber or in the joint region between two different fibers. Fiber-to-fiber coupling theory is discussed in this chapter by assuming a uniform mode power distribution in the fibers.

The optical power that can be coupled from one fiber to another is limited by the number of modes that can propagate in each fiber. The total number of modes in a fiber is [11]

$$N = k^2 \int_o^a \left[n^2(r) - n_2^2\right] r \, dr \qquad (3.1)$$

where $k=2\pi/\lambda$, $n(r)$ is the core refractive index profile, and n_2 is the refractive index of the cladding.
For graded index fiber with a power law profile,

$$n(r) = \begin{cases} n_1\left[1 - 2\Delta(\frac{r}{a})^{\alpha}\right]^{1/2} & \text{for } r < a \\ n_1(1 - 2\Delta)^{1/2} & \text{for } r > a \end{cases} \tag{3.2}$$

Local numerical aperture is define as [11]

$$NA(r) = \begin{cases} \left[n^2(r) - n_2^2\right]^{1/2} \simeq NA(0)\sqrt{1 - (\frac{r}{a})^{\alpha}} & \text{for } r < a \\ 0 & \text{for } r > a \end{cases} \tag{3.3}$$

where the axial numerical aperture is defined as

$$NA(0) = (n_1^2 - n_2^2)^{1/2} \tag{3.4}$$

Hence the total number of modes can be expressed as

$$N = k^2 NA^2(0) \int_o^a \left[1 - (\frac{r}{a})^{\alpha}\right] r \, dr \tag{3.5}$$

The fraction of energy coupled from one fiber to another is proportional to the common mode volume N_{comm}. The fiber-to-fiber coupling efficiency η_F is given by

$$\eta_F = \frac{N_{COMM}}{N_E} \tag{3.6}$$

where N_E is the number of modes in the emitting fiber. The fiber-to-fiber coupling loss L_F is given in terms of η_F as

$$L_F = -10 \log \eta_F \tag{3.7}$$

3.2 INTRINSIC PARAMETERS

Differences in the geometrical and waveguide characteristics of any two waveguides being joined can have a profound effect on fiber-to-fiber coupling efficiency. These differences include variations in core diameter, core area ellipticity, numerical aperture, refractive index profile, and core-cladding concentricity of each fiber.

The coupling efficiencies resulting from core diameter, numerical aperture, and core refractive-index profile mismatches can easily be found from Eqs.(3.5) and (3.6). Let the subscripts E and R refer to the emitting and receiving fibers, respectively. If the radii a_E and a_R of the two fibers to be joined are not equal but the axial numerical apertures and the index profiles are equal [i.e. $NA_E(0) = NA_R(0)$ and $\alpha_E = \alpha_R$], then the coupling efficiency is

$$\eta_F(a) = \left(\frac{a_R}{a_E}\right)^2 \quad \text{for} \quad a_R < a_E$$

$$\eta_F(a) = 1 \qquad \text{for} \quad a_R \geq a_E \tag{3.8}$$

It is very obvious that if $a_R > a_E$, all the power from the transmitting fiber is received by the receiving fiber.

If instead the radii and the index profiles of the two coupled fibers are identical but their axial numerical apertures are different, then

$$\eta_F(NA) = \left(\frac{NA_R(0)}{NA_E(0)}\right)^2 \qquad \text{for } NA_R(0) < NA_E(0)$$

$$\eta_F(NA) = 1 \qquad \text{for } NA_R(0) \geq NA_E(0) \tag{3.9}$$

Finally, if the radii and the axial numerical apertures are the same but the core refractive-index profiles differ in two joined fibers, then the coupling efficiency is

$$\eta_F(\alpha) = \frac{\alpha_R(\alpha_E + 2)}{\alpha_E(\alpha_R + 2)} \qquad \text{for } \alpha_R < \alpha_E$$

$$\eta_F(\alpha) = 1 \qquad \text{for } \alpha_R \geq \alpha_E \tag{3.10}$$

This results because for $\alpha_R < \alpha_E$ the number of modes that can be supported by the receiving fiber is less than the number

of modes in the emitting fiber. If $\alpha_R > \alpha_E$, then all modes in the emitting fiber can be captured by the receiving fiber.

The results stated in Eqs. (3.8), (3.9) and (3.10) are valid for both step-index and graded-index fibers. From these three equations, it can be noticed that the sensitivity of coupling efficiency to α mismatch is substantially less than that to numerical aperture or core radius mismatch.

Although generally less significant, other intrinsic mismatch parameters, such as core ellipticity and concentricity, do contribute to the total coupling loss. The total intrinsic coupling loss cannot be calculated as the sum of the losses due to the individual parameters mismatches. To properly obtain the combined effects to these parameters one must use the computer model described in [12].

3.3 EXTRINSIC PARAMETERS (STEP INDEX FIBERS)

Extrinsic fiber-to-fiber coupling efficiency factors include separation, angular tilt, axial offset (transverse offset) and fiber end quality.

The effect of separating the two fiber ends longitudinally by a gap S is shown in Figure 3.1. All the higher order mode optical power emitted in the ring of width x will not be intercepted by the receiving fiber. By assuming uniform mode power distribution, it is straightforward to show that, for a step-index fiber, the coupling efficiency in this case is

$$\eta_F = \left(\frac{a}{a + S \tan \theta_C}\right)^2 \tag{3.11}$$

where θc is the critical acceptance angle of the fiber. From eq. (3.11), it can be observed that the larger θc the greater the loss.

When the axes of two joined fibers are angularly misaligned at the joint, the optical power that leaves the emitting fiber outside of the solid acceptance angle of the receiving fiber will be lost. For two step-index fibers having an angular misalignment θ, the optical power coupling efficiency at the joint has been shown to be [13, 14].

$$\eta_F = \cos\theta \left\{\frac{1}{2} - \frac{1}{\pi} P(1 - P^2)^{1/2} - \frac{1}{\pi} \sin^{-1} P - q\left[\frac{1}{\pi} y(1 - y^2)^{1/2} + \frac{1}{\pi} \sin^{-1} y + \frac{1}{2}\right]\right\} \tag{3.12}$$

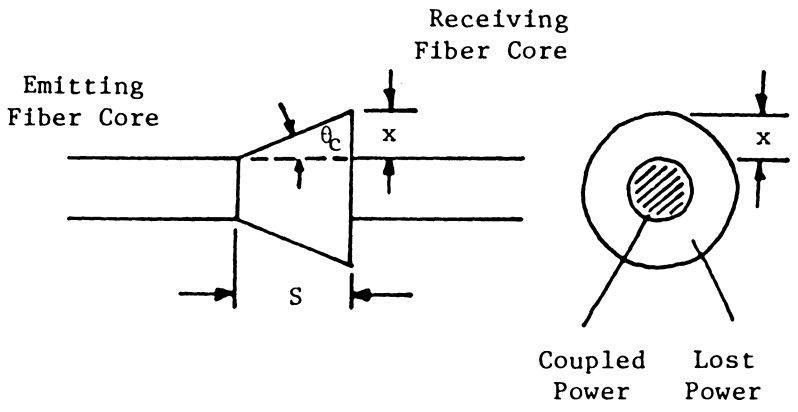

Figure 3.1. Loss effect when the fiber ends are separated longitudinally by a gap S.

where

$$P = \frac{\cos\theta_c(1 - \cos\theta)}{\sin\theta_c \sin\theta}$$

$$q = \frac{\cos^3\theta_c}{(\cos^2\theta_c - \sin^2\theta)^{3/2}}$$

$$y = \frac{\cos^2\theta_c(1 - \cos\theta) - \sin^2\theta}{\sin\theta_c \cos\theta_c \sin\theta}$$

The coupling efficiency due to angular misalignment is also dependent on θc. The values of p, q and y vary inversely with θc. Thus, coupling efficiency decreases if θc is smaller. The use of index matching fluid enhances the effect of angular misalignment because θc is smaller if n_o is larger in value. Physically, extrinsic loss attributable to angular misalignment only is impossible, since end separation must accompany angular misalignment.

To illustrate the effects of axial offset, let us first consider the simple case of two identical step-index fibers of core radii a. Suppose that their axes are offset by a separation d at their common junction, as is shown in Figure 3.2 . Since the numerical aperture is contant across the end faces of the two fibers, the optical power coupled from one

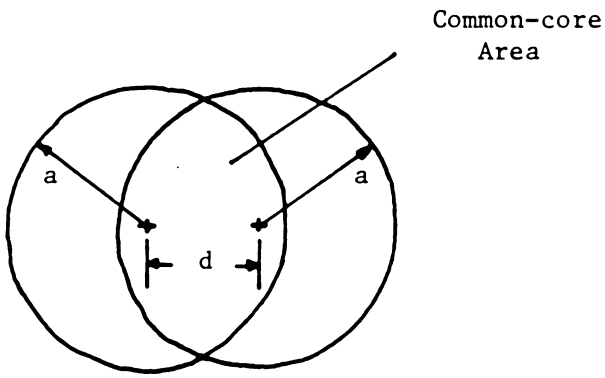

Figure 3.2. Axial offset reduces the common core area of the two fiber end faces.

fiber to another is simply proportional to the common area A_{comm} of the two fiber cores.

This common area is

$$A_{COMM} = 4 \int_{o}^{\theta_1} \int_{r_1}^{a} r \, dr \, d\theta$$

where the limits of integration shown in Figure 3.3 are

$$r_1 = \frac{d}{2 \cos \theta}$$

and $$\theta_1 = \text{arc cos } \frac{d}{2a}$$

After integration,

$$A_{COMM} = 2a^2 \text{ arc cos } \frac{d}{2a} - d(a^2 - \frac{d^2}{4})^{1/2}$$

Thus, the coupling efficiency is simply the ratio of the common core area to the core end face area

$$\eta_F = \frac{A_{COMM}}{\pi a^2} = \frac{2}{\pi} \text{ arc cos } \frac{d}{2a} - \frac{d}{\pi a} \left[1 - (\frac{d}{2a})^2\right]^{1/2} \qquad (3.13)$$

Fresnel reflections are other sources of coupling loss. Light is reflected at the glass-air interface at the exit of the emitting fiber and at the air-glass interface at the entrance to the receiving fiber.

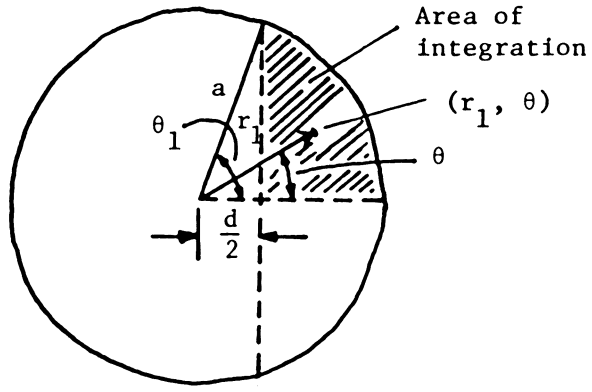

Figure 3.3. Area and limits of integration for the common core area of two parabolic graded-index fibers.

For step index fibers with core refractive index n_1, and a refractive index n_o of the medium between the fiber ends, the reflection coefficient for each interface is

$$R = \frac{(n_1 - n_o)^2}{(n_1 + n_o)^2} \tag{3.14}$$

For step index fibers with n_1=1.464, and n_o=1(air), then R is equal to 3.5%. Therefore, the maximaum coupling efficiency with an air gap between the fiber ends is approximately 93%.

Eliminating the air gap between the fiber ends by introducing an index matching medium (i.e.$n_o = n_1$) has two effects. These two effects are concentrating the emitting radiation into a smaller core (reduces θc) and reducing the reflection loss. These effects reduce the sensitivity of coupling efficiency to end separation. Fiber end defects such as rough areas or angled end surfaces will contribute to scatter and reflection losses. These losses are difficult to quantify. The use of an index matching medium will reduce their effects.

3.4 EXTRINSIC PARAMETERS (PARABOLIC GRADED INDEX FIBERS)

For graded index fibers, θc is a function of distance from the center of the core. Thus the calculation of coupling efficiency due to separation or angular misalignment is more complicated for these fibers [15,21].

The calculation of power coupled from one graded index fiber into another identical one is more complex since the numerical aperture varies across the fiber end face. If the end face of a graded index fiber is uniformly illuminated, the optical power accepted by the core will be the power that falls within the numerical aperture of the fiber. The optical power density p(r) at a point r on the fiber end is proportional to the square of the local numerical aperture NA(r) at that point [11] :

$$p(r) = p(o) \frac{NA^2(r)}{NA^2(o)} \tag{3.15}$$

The parameter p(0) is the power density at the core axis which is related to the total power P in the fiber by

$$P = \int_o^{2\pi} \int_o^a p(r) r \, dr \, d\theta \tag{3.16}$$

For a fiber with a parabolic index profile, the power density expression at a point r given by Eq. (3.15) becomes

$$p(r) = p(o)\left[1 - \left(\frac{r}{a}\right)^2\right] \tag{3.17}$$

Using Eqs.(3.16) and (3.17) the relationship between the axial power density p(0) and the total power P in the emitting fiber is

$$P = \frac{\pi a^2}{2} p(o) \tag{3.18}$$

Let us now calculate the power transmitted across the butt joint between the two graded index fibers with an axial offset d, as shown in Figure 3.4. The overlap region should be considered separately for the areas A_1 and A_2. In area A_1 the numerical aperture is limited by that of the emitting fiber, whereas in area A_2 the numerical aperture of the receiving fiber is smaller than that of the emitting fiber. The vertical dashed line separating the two areas is the locus of points where the numerical apertures are equal.

To determine the power coupled into the receiving fiber, the power density given by (3.17) is integrated separately over areas A_1 and A_2. Since the numerical aperture of the

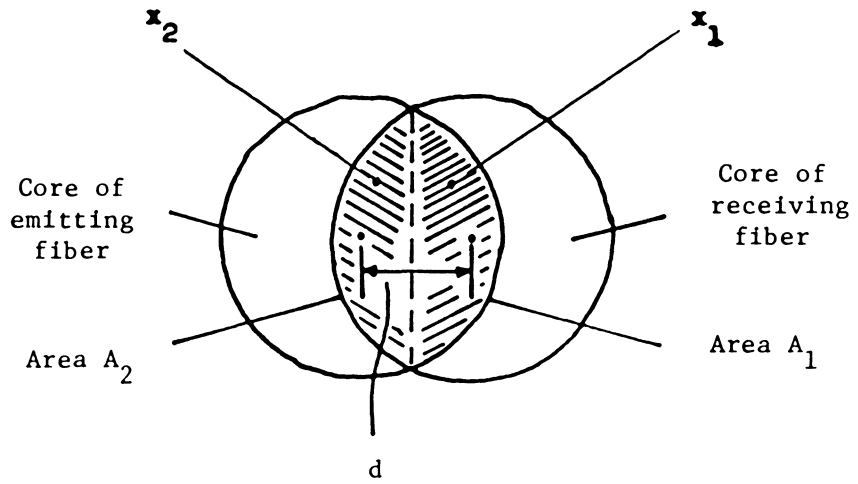

Figure 3.4. Core overlap region for two identical parabolic graded-index fibers with an axial separation d. Points x_1 and x_2 are arbitrary points of symmetry in areas A_1 and A_2.

emitting fiber is smaller than that of the receiving fiber in area A_1, all of the power emitted in this region will be accepted by the receiving fiber. The received power P_1 in area A_1 is, thus,

$$P_1 = 2\int_o^{\theta_1}\int_{r_1}^{a} p(r)r\,dr\,d\theta$$

$$= 2p(o)\int_o^{\theta_1}\int_{r_1}^{a}\left[1 - \left(\frac{r}{a}\right)^2\right]rdrd\theta \qquad (3.19)$$

where $r_1 = \dfrac{d}{2\cos\theta}$

and $\theta_1 = \arccos\dfrac{d}{2a}$

Carrying out the integration yields

$$P_1 = \frac{a^2}{2}\,p(o)\left\{\arccos\frac{d}{2a} - \left[1 - \left(\frac{d}{2a}\right)^2\right]^{1/2}\frac{d}{6a}\left(5 - \frac{d^2}{2a^2}\right)\right\} \qquad (3.20)$$

In area A_2 the emitting fiber has a larger numerical aperture than the receiving fiber. This means that the receiving fiber will accept only that fraction of the emitted optical power

that falls within its own numerical aperture. This power can be found easily from symmetry considerations. The numerical aperture of the receiving fiber at a point x_2 in area A_2 is the same as the numerical aperture of the emitting fiber at the symmetrical point x_1 in an area A_1.Thus the optical power accepted by the receiving fiber at any point x_2 in area A_2 is equal to that emitted from the symmetrical point x_1 in area A_1. The total power P_2 coupled across area A_2 is thus equal to the power P_1 coupled across area A_1. Combining these results, we have that the total power P_o accepted by the receiving fiber is $P_o = 2P_1$ [11]. Thus,

$$\eta_F = \frac{P_o}{P} = \frac{2}{\pi}\left\{\arccos\frac{d}{2a} - \left[1 - \left(\frac{d}{2a}\right)^2\right]^{1/2}\frac{d}{6a}\left(5 - \frac{d^2}{2a^2}\right)\right\} \qquad (3.21)$$

Measured coupling losses in dB as a function of normalized mechanical misalignments are shown in Figure 3.5 [16] for the two different experimental cases. The axial offset d and the separation s have been normalized to the fiber core radius a. The angular misalignment θ is normalized to the on axis NA.

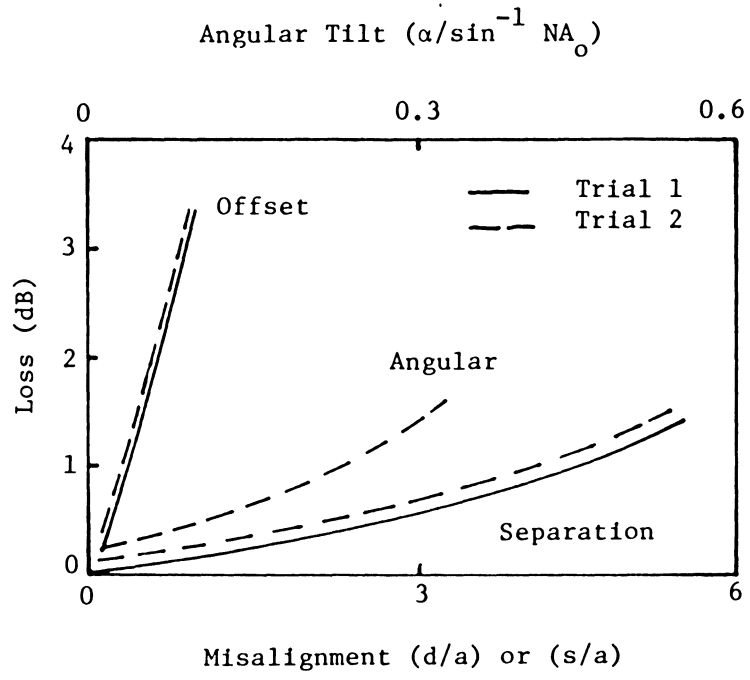

Figure 3.5. Experimental comparison of loss (in dB) as a function of mechanical misalignments.

In the first experiment, a 1.8m section of fiber was used. The fiber core diameter was 50μm with a 100μm overall diameter. In the second experiment, a 20m section of fiber with 55μm diameter core and a 100μm outside diameter was used. Both fibers had a parabolic graded index with on axis NA of 0.20. In both cases, index matching fluid was applied to the joints.

The measured results clearly show that coupling efficiency is most sensitive to transverse offset. This great sensitivity to transverse offset can be used in applications such as fiber optic sensors. In the next chapter, the coupling efficiency of fibers due to transverse offset is studied in more detail.

CHAPTER IV

FIBER-TO-FIBER COUPLING EFFICIENCY DUE TO TRANSVERSE OFFSET

4.1 TRANSVERSE OFFSET OF PARABOLIC GRADED INDEX FIBER WITH CENTRAL DIP.

The sensitivity of microbend fiber optic sensors is increased by using parabolic graded index fibers with a central dip [6]. It is thus interesting to study whether the sensitivity of transverse offset fiber optic sensors also is increased by using such parabolic graded index fibers. The coupling efficiency of this type of fiber is derived in this section by assuming a uniform mode power distribution.

The refractive index profile of a parabolic graded index fiber with central dip can be expressed as

$$n(r) = \begin{cases} n_3 \sqrt{1 + \varepsilon \frac{r}{a}} , & 0 < r < b \\ n_1 \sqrt{1 - 2\Delta(\frac{r}{a})^2} , & b < r < a \\ n_1 \sqrt{1 - 2\Delta} \simeq n_2 , & r > a \end{cases} \qquad (4.1)$$

where $$\varepsilon = \frac{a}{b}\left\{\frac{n_1^2}{n_3^2}\left[1 - 2\Delta\left(\frac{b}{a}\right)^2\right] - 1\right\}$$

This profile is shown in Figure 4.1. The optical power density p(r) at a point r on the fiber end is [9]

$$p(r) = P_m \frac{n^2(r) - n_2^2}{n_m^2 - n_2^2} \tag{4.2}$$

where P_m is the power density at points r=b. For d>2b, the coupling efficiency is more or less the same as Eq. (3.21). Let us consider a small offset such that d<2b.

The power in the emitting fiber is

$$P = \int_0^{2\pi}\int_0^{a} p(r) r \, dr \, d\theta$$

$$= \int_0^{2\pi}\int_0^{b} P_1(r) r \, dr \, d\theta + \int_0^{2\pi}\int_b^{a} P_2(r) r \, dr \, d\theta \tag{4.3}$$

where

$$P_1(r) = P_m \frac{\left(n_3\sqrt{1 + \varepsilon\frac{r}{a}}\right)^2 - n_2^2}{n_m^2 - n_2^2}$$

and $$P_2(r) = P_m \frac{\left(n_1\sqrt{1 - 2\Delta\left(\frac{r}{a}\right)^2}\right)^2 - n_2^2}{n_m^2 - n_2^2}$$

After some manipulations, the power can be expressed as

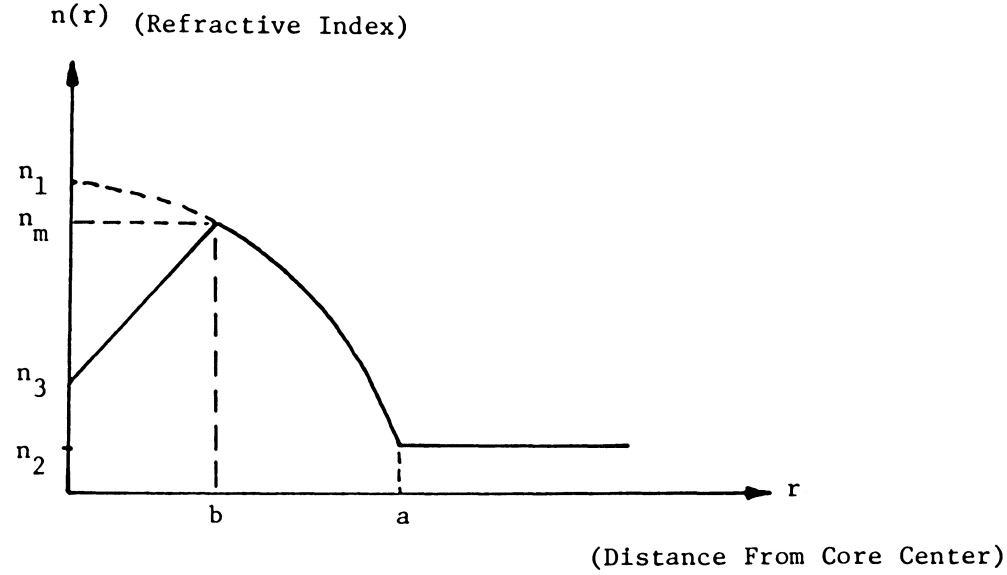

Figure 4.1. The refractive index profile of a parabolic graded index fiber with central dip.

$$P = \frac{P_m}{n_m^2 - n_2^2} \cdot 2\pi \left\{ \frac{n_3^2 \varepsilon}{a} \frac{b^3}{3} + (n_3^2 - n_1^2) \frac{b^2}{2} + \frac{a^2}{4} (n_1^2 - n_2^2) + \frac{n_1^2 \Delta}{2a^2} b^4 \right\} \quad (4.4)$$

For the sake of simplicity, let us assume that the light accepted by the receiving fiber at areas A_3 and A_4 has power density of $P_2(r)$ (see Figure 4.2). This is not true in the actual case. Thus the total power accepted by the receiving fiber is

$$P_o = 4\left\{ \int_o^{\theta_1} \int_{\frac{d}{2\cos\theta}}^{a} P_2(r) r dr d\theta - \int_o^{\theta_2} \int_{\frac{d}{2\cos\theta}}^{b} P_2(r) r dr d\theta + \int_o^{\theta_2} \int_{\frac{d}{2\cos\theta}}^{b} P_1(r) r dr d\theta \right\} \quad (4.5)$$

where $\theta_1 = \cos^{-1} \frac{d}{2a}$

and

$$\theta_2 = \cos^{-1} \frac{d}{2b}$$

Carrying out the integrations yields

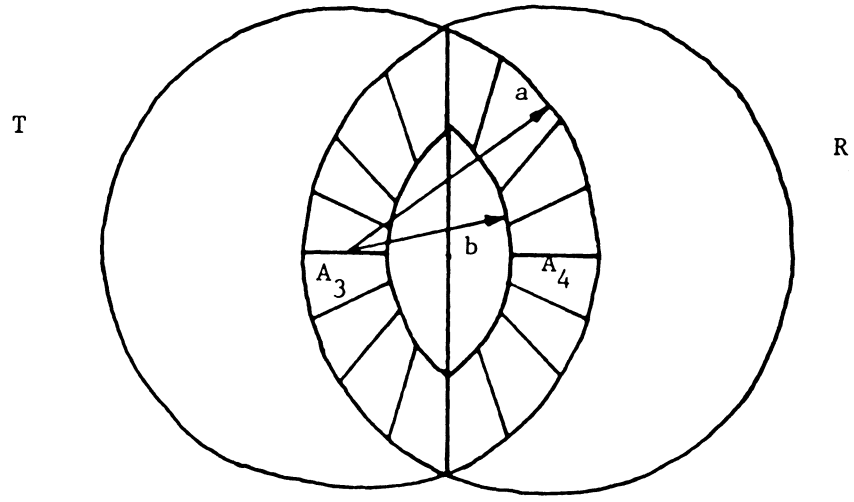

Figure 4.2. Common core area of two parabolic graded-index fibers with central dip.

$$\int_0^{\theta_1}\int_{\frac{d}{2\cos\theta}}^{a} P_2(r)\,r\,dr\,d\theta$$

$$= \frac{2P_m}{n_m^2 - n_2^2}\left\{\frac{a^2}{2}\left[n_1^2(1-\Delta) - n_2^2\right]\theta_1 - \frac{n_1^2 - n_2^2}{8}\,d^2\tan\theta_1 + \frac{n_1^2\Delta d^4}{96a^2}\tan\theta_1(\sec^2\theta_1 + 2)\right\} \tag{4.6}$$

$$\int_0^{\theta_2}\int_{\frac{d}{2\cos\theta}}^{b} P_2(r)\,r\,dr\,d\theta$$

$$= \frac{P_m}{n_m^2 - n_2^2}\left\{\left(\frac{n_1^2 - n_2^2}{2}\,b^2 - \frac{n_1^2\Delta}{2a^2}\,b^4\right)\theta_2 - \frac{n_1^2 - n_2^2}{8}\,d^2\tan\theta_2 + \frac{n_1^2\Delta d^4}{96a^2}\tan\theta_2(\sec^2\theta_2 + 2)\right\} \tag{4.7}$$

and

$$\int_0^{\theta_2}\int_{\frac{d}{2\cos\theta}}^{b} P_1(r)\,r\,dr\,d\theta$$

$$= \frac{P_m}{n_m^2 - n_2^2}\left\{\left(\frac{n_3^2 - n_2^2}{2}\,b^2 + \frac{\varepsilon n_3^2}{3a}\,b^3\right)\theta_2 - \frac{n_3^2 - n_2^2}{8}\,d^2\tan\theta_2 - \frac{\varepsilon n_3^2 d^3}{48a}\left[\sec\theta_2\tan\theta_2 + \ln(\sec\theta_2 + \tan\theta_2)\right]\right\} \tag{4.8}$$

Note that,

$$\tan \theta_1 = \frac{2a}{d}\sqrt{1 - \left(\frac{d}{2a}\right)^2} \qquad \sec \theta_1 = \frac{2a}{d}$$

$$\tan \theta_2 = \frac{2b}{d}\sqrt{1 - \left(\frac{d}{2b}\right)^2} \qquad \sec \theta_2 = \frac{2b}{d}$$

Thus, the coupling efficiency for parabolic graded index fibers with central dip due to transverse offset of $d<2b$ is

$$\eta = \frac{P_o}{P}$$

where P is shown in Eq.(4.4)

and

$$P_o = \frac{4P_m}{n_m^2 - n_2^2}\left\{\frac{1}{4}(n_1^2 - n_2^2)\left[a^2\theta_1 + \frac{1}{6}\sqrt{1 - \left(\frac{d}{2a}\right)^2}\left(\frac{d^3}{2a} - 5ad\right)\right]\right.$$

$$- \left[\left(\frac{n_1^2 - n_3^2}{2}b^2 - \frac{n_1^2\Delta}{2a^2}b^4\right)\theta_2 + \frac{n_1^2\Delta d^3 b}{24a^2}\sqrt{1 - \left(\frac{d}{2b}\right)^2}\left(\frac{2b^2}{d^2} + 1\right)\right]$$

$$+\left[\frac{\varepsilon n_3^2}{3a}b^3\theta_2 - \frac{n_3^2 - n_1^2}{4}bd\sqrt{1 - \left(\frac{d}{2b}\right)^2} - \frac{\varepsilon n_3^2 d^3}{48a}\left[\frac{4b^2}{d^2}\sqrt{1 - \left(\frac{d}{2b}\right)^2}\right.\right.$$

$$\left.\left.\left.+ \ln\left(\frac{2b}{d} + \frac{2b}{d}\sqrt{1 - \left(\frac{d}{2b}\right)^2}\right)\right]\right]\right\} \qquad (4.9)$$

where

$$\theta_1 = \cos^{-1} \frac{d}{2a}$$

and $$\theta_2 = \cos^{-1} \frac{d}{2b}$$

For an ITT parabolic graded-index fiber with a central dip, the parameters are

$n_1 = 1.486$

$n_2 = 1.450$

$n_3 = 1.453$

$a = 52\mu m$

$b = 21\mu m$

The coupling efficiency versus axial offset is plotted in Figure 4.3 by using these data. The sensitivity of the parabolic graded-index fiber without a central dip is better than that of the central dipped fiber.

4.2 TRANSVERSE OFFSET OF GRADED INDEX FIBERS WITH DIFFERENT VALUES OF α

The sensitivity of coupling efficiency of graded index fibers to transverse offset is studied in this section as α

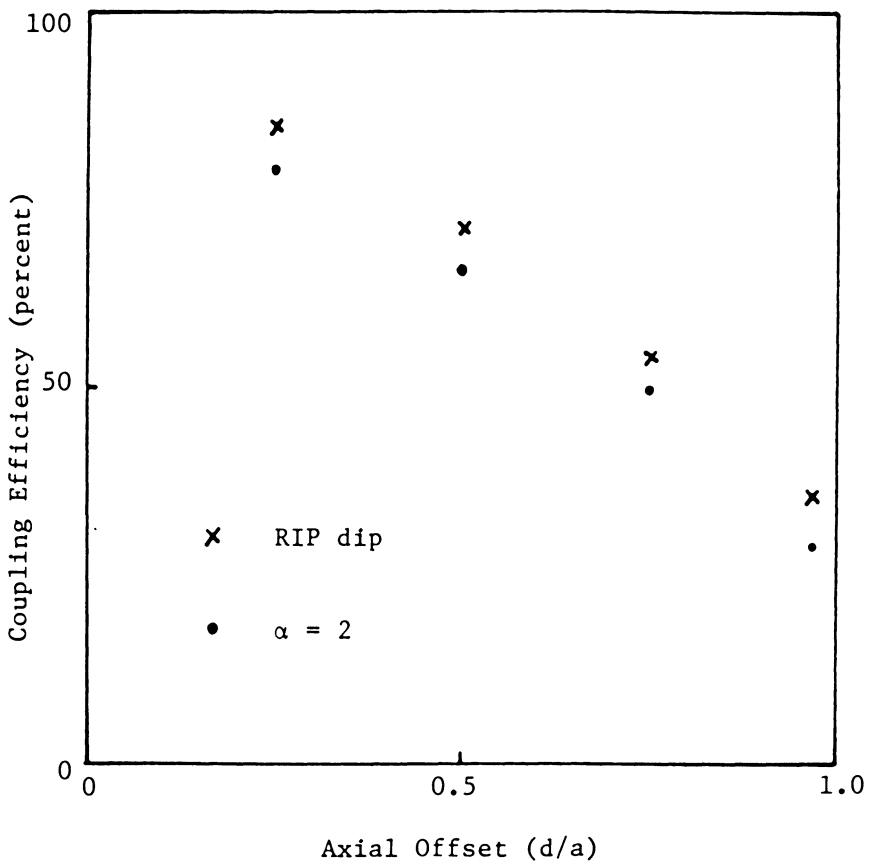

Figure 4.3. Comparison of coupling efficiency as a function of axial offset for parabolic graded-index fibers with and without central dip.

varies. Linear equations of coupling efficiency are derived for small transverse offset.

Let us first derive a general equation for the power emitted from the emitting fiber for different α values. The emitted power is

$$P = \int_0^{2\pi}\int_0^a p(o)\left[1 - \left(\frac{r}{a}\right)^{\alpha}\right] r\, dr\, d\theta$$

$$= \frac{\alpha}{\alpha + 2}\, \pi a^2 p(o) \qquad (4.10)$$

Since a closed form solution in α is difficult and only the potential variation in coupling versus α is to be analyzed, several specific values of α will be considered.

For example, if $\alpha = 1$, $P_{E_1} = 2\pi a^2 p(0)/3$

Assuming $r_1 = d/2\cos\theta$ and $\theta_1 = \cos^{-1}(d/2a)$, thus, the received power is

$$P_{R_1} = 4\int_0^{\theta_1}\int_{r_1}^a p(o)\left[1 - \frac{r}{a}\right] r\, dr\, d\theta$$

$$= 4p(o)\left\{\frac{a^2}{6}\,\theta_1 - \int_0^{\theta_1}\left(\frac{d^2}{8\cos^2\theta} - \frac{d^3}{24a\cos^3\theta}\right) d\theta\right\}$$

$$= 4p(o)\left\{\frac{a^2}{6}\,\theta_1 - \frac{d^2}{8}\tan\theta_1 + \frac{d^3}{24a}\left[\frac{1}{2}\sec\theta\tan\theta + \frac{1}{2}\ln(\sec\theta + \tan\theta)\right]_o^{\theta_1}\right\}$$

$$= 4p(o)\left\{\frac{a^2}{6}\cos^{-1}\frac{d}{2a} - \frac{d^2}{8}\frac{2a}{d}\sqrt{1 - \left(\frac{d}{2a}\right)^2} + \frac{d^3}{48a}\left[\frac{4a^2}{d^2}\sqrt{1 - \left(\frac{d}{2a}\right)^2} + \ln\left(\frac{2a}{d} + \frac{2a}{d}\sqrt{1 - \left(\frac{d}{2a}\right)^2}\right)\right]\right\}$$

$$= \frac{2}{3}\,p(o)a^2\left\{\cos^{-1}\frac{d}{2a} - \frac{d}{a}\sqrt{1 - \left(\frac{d}{2a}\right)^2} + \frac{d^3}{8a^3}\ln\left(\frac{2a}{d} + \frac{2a}{d}\sqrt{1 - \left(\frac{d}{2a}\right)^2}\right)\right\} \qquad (4.11)$$

Thus coupling efficiency, for $\alpha = 1$ is then

$$\eta_1 = \frac{P_{R_1}}{P_{E_1}}$$

$$= \frac{2}{\pi}\left\{\cos^{-1}\frac{d}{2a} - \frac{d}{a}\sqrt{1 - \left(\frac{d}{2a}\right)^2} + \frac{d^3}{8a^3}\ln\left(\frac{2a}{d} + \frac{2a}{d}\sqrt{1 - \left(\frac{d}{2a}\right)^2}\right)\right\} \qquad (4.12)$$

When the transverse offset d is small compared to the core radius a,

$$\cos^{-1}\frac{d}{2a} \simeq \frac{\pi}{2} - \frac{d}{2a} \quad \text{and} \quad \left[1 - \left(\frac{d}{2a}\right)^2\right]^{1/2} \simeq 1 - \frac{1}{2}\left(\frac{d}{2a}\right)^2$$

By neglecting the higher order terms, for small transverse offset we get,

$$\eta_1 = 1 - \frac{3}{\pi}\frac{d}{a} \tag{4.13}$$

which is a linear equation.

If instead $\alpha = 3$, the receiving power is

$$P_{R_3} = 4\int_o^{\theta_1}\int_{r_1}^{a} p(o)\left[1 - (\frac{r}{a})^3\right] rdrd\theta$$

$$= 4p(o)\left\{\frac{3}{10}a^2\theta_1 - \frac{d^2}{8}\tan\theta_1 + \frac{d^5}{2^5 \cdot 5a^3}\left[\frac{1}{4}\tan\theta_1 \sec^3\theta_1 + \frac{3}{4}(\frac{1}{2}\sec\theta_1\tan\theta_1 + \frac{1}{2}\ln|\sec\theta_1 + \tan\theta_1|)\right]\right\}$$

$$= \frac{6}{5}p(o)a^2\left\{\cos^{-1}\frac{d}{2a} - \frac{3}{4}\frac{d}{a}\sqrt{1 - (\frac{d}{2a})^2} + \frac{1}{2^5}\frac{d^3}{a^3}\sqrt{1 - (\frac{d}{2a})^2} + \frac{1}{2^7}\frac{d^5}{a^5}\ln(\frac{2a}{d} + \frac{2a}{d}\sqrt{1 - (\frac{d}{2a})^2})\right\} \tag{4.14}$$

The power emitted from the emitting fiber is then

$$P_{E_3} = \frac{3}{5}\pi a^2 p(o) \tag{4.15}$$

Thus the coupling efficiency in this case is

$$\eta_3 = \frac{P_{R_3}}{P_{E_3}}$$

$$= \frac{2}{\pi}\left\{\cos^{-1}\frac{d}{2a} - \frac{3}{4}\frac{d}{a}\sqrt{1 - (\frac{d}{2a})^2} + \frac{1}{2^5}\frac{d^3}{a^3}\sqrt{1 - (\frac{d}{2a})^2}\right.$$

$$\left. + \frac{1}{2^7}\frac{d^5}{a^5}\ln\left(\frac{2a}{d} + \frac{2a}{d}\sqrt{1 - (\frac{d}{2a})^2}\right)\right\} \qquad (4.16)$$

For small offset, η_3 can be simplified to

$$\eta_3 = 1 - \frac{5}{2\pi}\frac{d}{a} \qquad (4.17)$$

Now, let us consider possible values of α which are smaller than 1. For $\alpha = 0.8$, the receiving power is

$$P_{R_{0.8}} = 4\int_o^{\theta_1}\int_{r_1}^{a} p(o)\left[1 - (\frac{r}{a})^{0.8}\right] r dr d\theta$$

$$= 4p(o)\int_o^{\theta_1}\left[\frac{1}{7}a^2 - \frac{r_1^2}{2} + \frac{5}{14}(\frac{d}{2})^{14/5} \times \right.$$

$$\left. \frac{1}{a^{4/5}}\sec^{14/5}\theta\right] d\theta$$

$$= 4p(o)\left\{\frac{1}{7}a^2\theta_1 - \frac{d^2}{8}\tan\theta_1 + \frac{5}{14}\left(\frac{d}{2}\right)^{14/5}\frac{1}{a^{4/5}}\left[\frac{5}{9}\sec^{4/5}\theta\tan\theta + \frac{4}{9}\int_o^{\theta_1}\sec^{4/5}\theta d\theta\right]\right\}$$

$$= 4p(o)a^2\left\{\frac{1}{7}\theta_1 - \frac{1}{4}\frac{d}{a}\sqrt{1 - \left(\frac{d}{2a}\right)^2} + \frac{5}{14}\left(\frac{d}{2a}\right)^{14/5}\left[\frac{5}{9}\left(\frac{2a}{d}\right)^{9/5} \times \sqrt{1 - \left(\frac{d}{2a}\right)^2} + \frac{4}{9}\int_o^{\theta_1}\sec^{4/5}\theta d\theta\right]\right\} \qquad (4.18)$$

Since $\sec^{4/5}\theta \leq \sec\theta$ for all values of θ,

thus $\int_o^{\theta_1}\sec^{4/5}\theta d\theta \leq \ln(\sec\theta_1 + \tan\theta_1)$

where $\ln(\sec\theta_1 + \tan\theta_1) = \ln\left[\frac{2a}{d} + \frac{2a}{d}\sqrt{1 - \left(\frac{d}{2a}\right)^2}\right]$

Hence we can observe that the term

$$\frac{5}{14}\left(\frac{d}{2a}\right)^{14/5} \times \frac{4}{9}\int_o^{\theta_1}\sec^{4/5}\theta d\theta$$

is much smaller than the other terms, and thus can be neglected.

Thus,

$$P_{R_{0.8}} = \frac{4}{7} a^2 p(o) \left\{ \text{arc cos } \frac{d}{2a} - \frac{19}{18} \frac{d}{a} \sqrt{1 - \left(\frac{d}{2a}\right)^2} \right\} \tag{4.19}$$

From Eq.(4.10), we get,

$$P_{E_{0.8}} = \frac{2\pi a^2 p(o)}{7}$$

Thus,

$$\eta_{0.8} = \frac{P_{R_{0.8}}}{P_{E_{0.8}}}$$

$$= \frac{2}{\pi} \left\{ \text{arc cos } \frac{d}{2a} - \frac{19}{18} \frac{d}{a} \sqrt{1 - \left(\frac{d}{2a}\right)^2} \right\} \tag{4.20}$$

For small transverse offset,

$$\eta_{0.8} = 1 - \frac{28}{9\pi} \frac{d}{a} \tag{4.21}$$

For $\alpha = 0.5$,

$$P_{R_{0.5}} = 4 \int_o^{\theta_1} \int_{r_1}^{a} p(o) \left[1 - \left(\frac{r}{a}\right)^{1/2} \right] r dr d\theta$$

$$= \frac{2a^2}{5} p(o) \left\{ \text{arc cos } \frac{d}{2a} - \frac{7}{6} \frac{d}{a} \sqrt{1 - \left(\frac{d}{2a}\right)^2} \right\} \tag{4.22}$$

and

$$P_{E_{0.5}} = \frac{\pi}{5} a^2 p(o) \tag{4.23}$$

Thus the coupling efficiency is

$$\eta_{0.5} = \frac{P_{R_{0.5}}}{P_{E_{0.5}}}$$

$$= \frac{2}{\pi}\left\{\arccos\frac{d}{2a} - \frac{7}{6}\frac{d}{a}\sqrt{1 - \left(\frac{d}{2a}\right)^2}\right\} \tag{4.24}$$

For small transverse offset, we have

$$\eta_{0.5} = 1 - \frac{10}{3\pi}\frac{d}{a} \tag{4.25}$$

Similarly, we can obtain the coupling efficiency of step index and parabolic graded index fibers for small transverse offset as

$$\eta_{\infty} = 1 - \frac{2}{\pi}\frac{d}{a} \tag{4.26}$$

$$\eta_2 = 1 - \frac{8}{3\pi}\frac{d}{a} \tag{4.27}$$

By observing Eqs (4.13), (4.17), (4.21), (4.25), (4.26) and (4.27) a general equation for the coupling efficiency of fi-

bers with refractive index profile α due to small transverse offset is obtained as follows,

$$\eta = 1 - \frac{2}{\pi} \frac{\alpha + 2}{\alpha + 1} \frac{d}{a} \tag{4.28}$$

This is a linear relationship between the coupling efficiency and the normalized transverse offset, d/a. This relationship is desirable in the applications of fiber optic sensors.

From Eq.(4.28), we can observe that the coupling efficiency is reduced if the value of α decreases. This means that the sensitivity of the transverse offset fiber optic sensor can be increased by using graded index fibers with a smaller value of α.

The plot of coupling efficiency versus axial offset is shown in Figure 4.4 for different values of α.

As shown in Figure 4.5, as the α of a fiber becomes smaller than 1 and keeps on decreasing towards zero, eventually its refractive index profile can allow only one propagating mode; this means it eventually becomes a single mode fiber. It is apparent that single mode fiber has great sen-

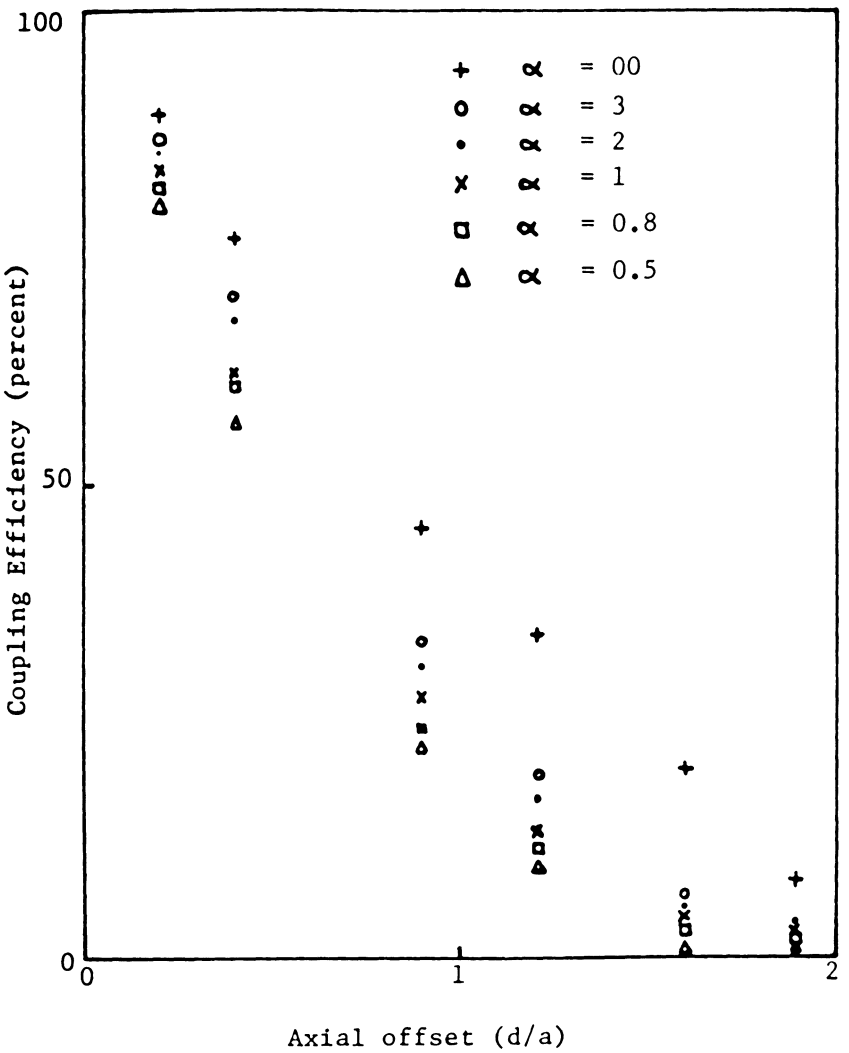

Figure 4.4. Coupling efficiency versus axial offset for different values of α.

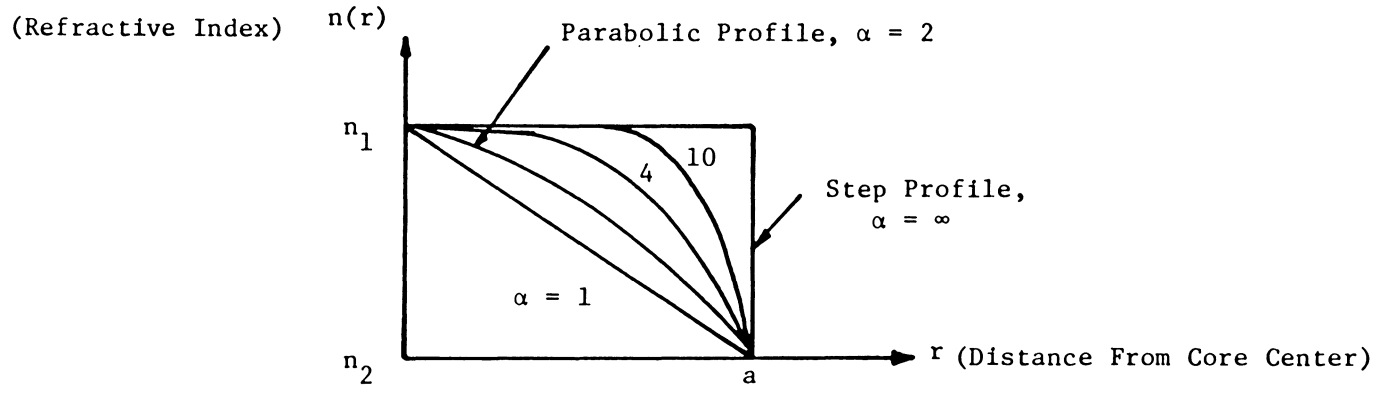

Figure 4.5. Power-law refractive index profile.

sitivity in coupling efficiency due to axial offset. A very small axial offset will cause the loss of a great amount of power. This will create some difficulties for using as fiber sensors. To suit one's purpose, a particular value of α can be chosen so that the fiber is easy to apply as an axial offset fiber optic sensor and at the same time exhibits good sensitivity.

4.3 EFFECTS OF LAUNCH BEAM NUMERICAL APERTURE

Fiber-to-fiber coupling efficiency depends strongly upon the power distribution in the emitting fiber. This in turn depends on the nature of the source, the launching conditions used to excite the fiber and the length of fiber between the source and the splice. These factors make the problem even more complicated.

Short fiber lengths are used in most fiber sensors, and a nonsteady state power distribution is encountered. Thus a knowledge of the effects of launching conditions on coupling efficiency is important. An experimental investigation of such effects of launch beam numerical aperture on optical fiber waveguide was presented by R. B. Kummer [17].

The receiving fiber length in the experiment was ~ 1m, while both long (900m) and short (~ 1m) emitting fiber lengths were studied. The NA and α of the fibers are 0.21 and 2.2, respectively. The transverse offset coupling efficiency for several different launch beam NAs was measured. The results are shown in Figure 4.6. The dotted curve is for the case of a long emitting fiber, where the coupling efficiency is insensitive to launch NA; the other curves are for a short (1m) emitting fiber. These data were all taken with the launch beam centered on the fiber core.

Several conclusions may be drawn from the data in Figure 4.6 . First, for offsets of less than about 1.1 core radii, the coupling efficiency variation as a function of transverse offset with a short emitting fiber is significantly reduced when using a launch NA which is much less than the fiber NA. A small launch NA excites primarily the low order fiber modes which propagate near the center of the fiber core, and these modes are least affected by small offsets. For offsets much greater than one core radius, however, this situation is reversed. Also, increasing the launch NA beyond the fiber NA is shown to have very little effect on the coupling efficiency.

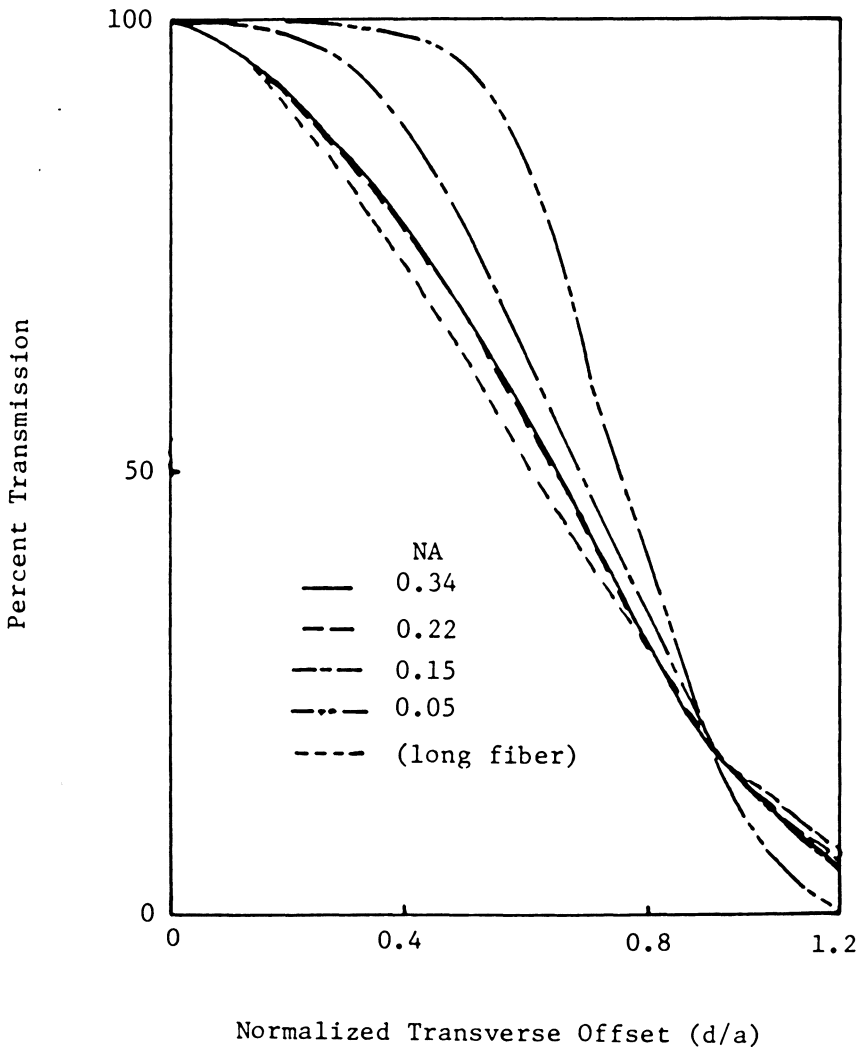

Figure 4.6. Coupling efficiency versus axial offset for various input conditions [17].

The second important observation is that, for offsets of less than about 1.1 core radii, the coupling efficiency measured with a long emitting fiber is smaller than that measured at any NA with a short emitting fiber. This result suggests that by launching on-axis with a Gaussian beam, only meridonal fiber modes are excited, while the steady state power distribution in the long emitting fiber contains additional higher order skew modes which can significantly affect the coupling efficiency.

In an attempt to launch more skew modes into a short emitting fiber , measurements were made with the launch beam displaced or tilted with respect to the fiber axis. Indeed,either of these was found to reduce the measured coupling efficiency. The magnitude of this effect depends upon many factors, but generally a launch beam displacement of ~0.5 core radii or an angular misalignment of ~3 degrees results in a 10 to 30 percent in sensivitity, depending on the offset [17].

4.4 DISCUSSION

The fiber-to-fiber coupling problem has been investigated in depth in both theoretical and experimental works by

several researchers [18,19,20,21,22,23,24,25]. Due to the complications caused by power distribution and launching conditions, some of the reported results do not seem agree with each other at first glance [21].

The authors in references [19,21] suggest that calculations of coupling efficiency based on uniform power distribution can estimate coupling efficiency of short fibers better than that of long fibers, and these results are not suitable for direct application to fiber optic transmission lines.

This is apparent because a steady state mode distribution is realized after propagation along a long fiber, where most of the energy is concentrated in the low order fiber modes. In this case, slight mechanical misalignments of the two joined fibers do not contribute significantly to joint loss. Thus the losses measured with a short fiber should be nearer to the theoretical value than those with a long fiber if the fibers are uniformly excited.

This suggestion seems in contradiction with the results shown in FIgure 4.7 [20] at first.From Figure 4.7 we can see that the losses measured with a 500m long fiber is nearer

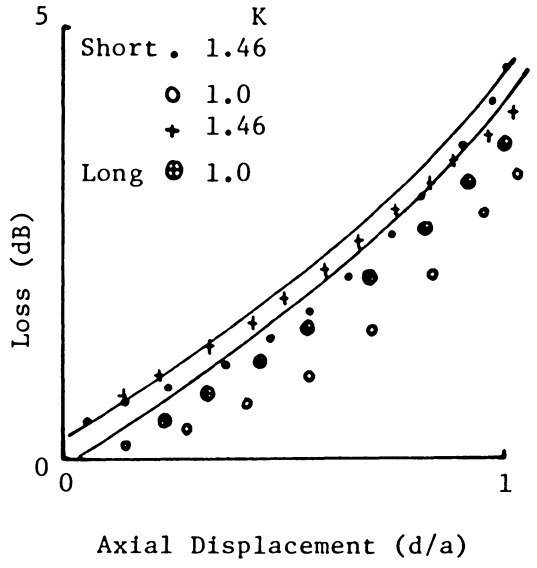

Figure 4.7. Loss versus axial offset for step-index fibers.

to the theoretical value than those with a 3m fiber. The reason for this contradiction is that the fibers in this experiment are excited by a He-Ne laser beam, which is not a uniform light source. Whereas the suggestion made in the references [19,21] is based on assuming that the fibers are uniformly excited. Halogen lamps or LEDs should be more appropriate for applications as uniform light sources.

CHAPTER V

EXPERIMENTS

This chapter describes measurements of fiber-to-fiber coupling efficiency versus fiber end separation and axial offset. The construction of an axial offset fiber sensor is also described.

5.1 COUPLING EFFICIENCY MEASUREMENTS

Step index fibers with a core diameter of 51μm and an NA of 0.2 were used in the experiment. The indices of refraction of the core and cladding of the fibers were 1.463 and 1.450, respectively. Both emitting and receiving fibers were ~ 1m in length.

A He-Ne laser was used as the light source. A microscope objective with a 10x/0.25 NA was used to collect and focus the light into the emitting fiber. Alignment was achieved by using micropositioners. The output of the receiving fiber was detected by an optical power meter. Mode strippers (liquid with a refractive index slightly higher than the cladding index) were used on both the emitting and receiving fibers

to eliminate cladding modes. The measurement setup is shown in Figure 5.1.

The experiment began by optimizing the power output from the fibers. The fibers were aligned using the micropositioners. The measurement of coupling efficiency versus separation was done by separating one fiber end with respect to the other by known distances and measuring the power output of the receiving fiber. This was repeated at normalized separations of ½ to 9 at an increament of ½ each time. The normalized separation is defined as s/a, where s is the longitudinal separation between the fiber ends and a is the core radius.

Similarly, the coupling efficiency versus axial offset measurement was done by offseting one fiber end with respect to the other by known amounts and recording the power output of the receiving fiber. This was repeated at normalized axial offsets of 0.2 to 2 at an increment of 0.2 each time. The normalized axial offset is defined as d/a.

The experiment was repeated by using same type of fiber and with same emitting and receiving fiber lengths. The results obtained in the two experiments are similar and are

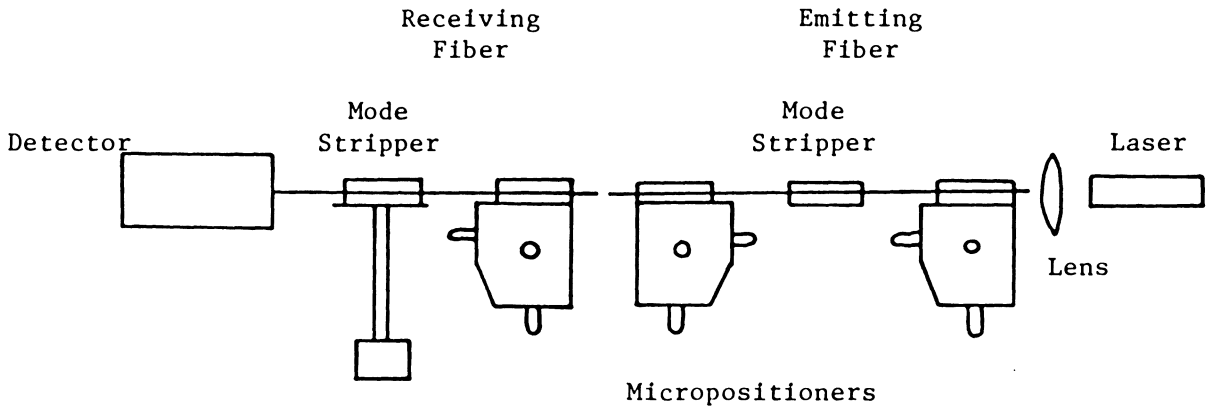

Figure 5.1. Coupling efficiency versus fiber end misalignment measurement setup.

shown in Figure 5.2 and Figure 5.3.From both Figure 5.2 and Figure 5.3, it can be observed that coupling efficiency is linearly decaying for small separation and axial offset. The coupling efficiency is definitely more sensitive to axial offset than separation.

The coupling efficiency obtained in the experiments is somewhat lower than in the case when only one extrinsic parameter is present. This may be caused by small angular misalignments usually present when measuring the coupling efficiency versus separation or axial offset.

5.2 CONSTRUCTION OF AN AXIAL OFFSET FIBER SENSOR

The construction of an axial offset fiber sensor is shown in Figure 5.4. This setup is basically the same as that in Figure 5.1, except there are a small aluminium block, an aluminium rod and a small box for adding weights. The same type of fiber is used in this setup as that shown in Figure 5.1.

The top surface of the aluminium block is a square of side 3 cm long. It was made such that a half of the area had a top surface which was slightly higher than the surface of

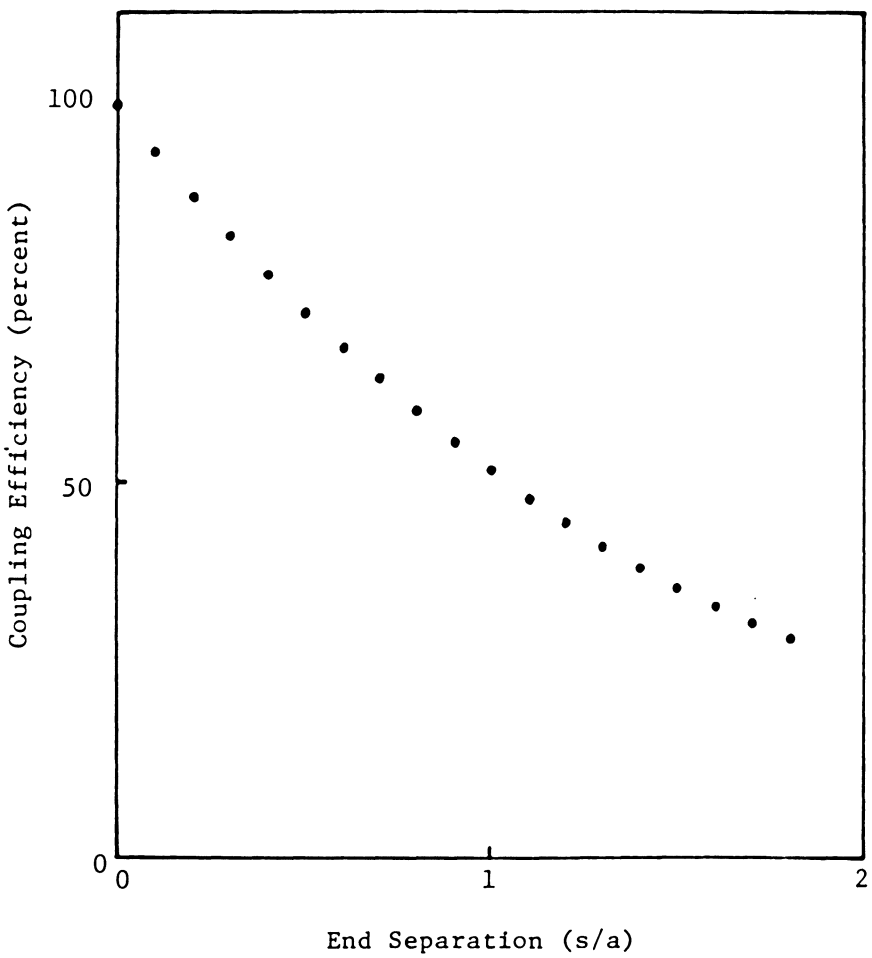

Figure 5.2.a. Coupling efficiency versus fiber end separation, first experiment.

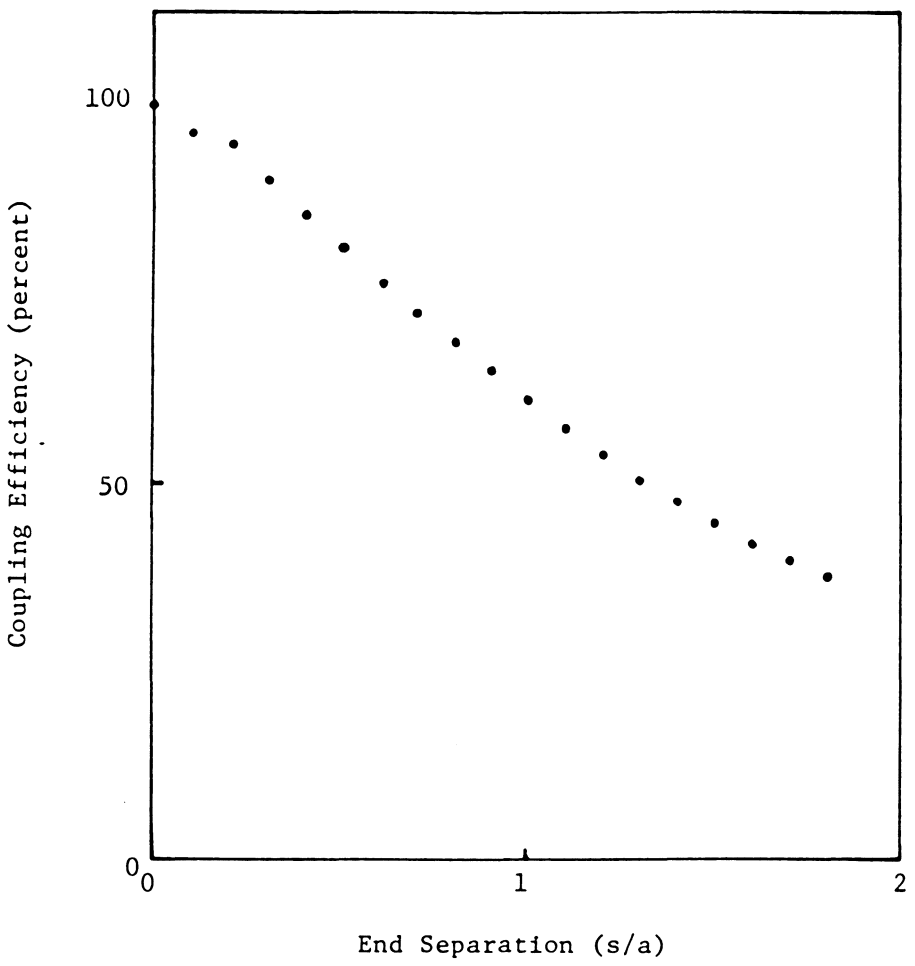

Figure 5.2.b. Coupling efficiency versus fiber end separation; second experiment.

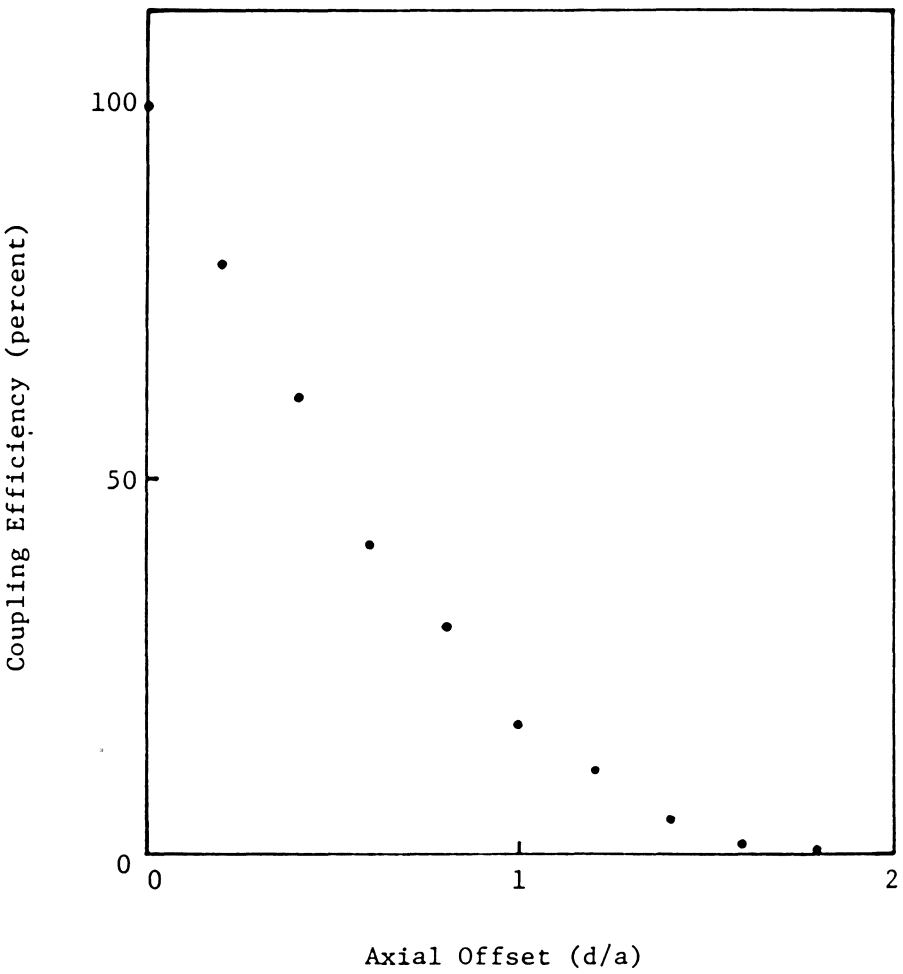

Figure 5.3.a. Coupling efficiency versus fiber axial offset; first experiment.

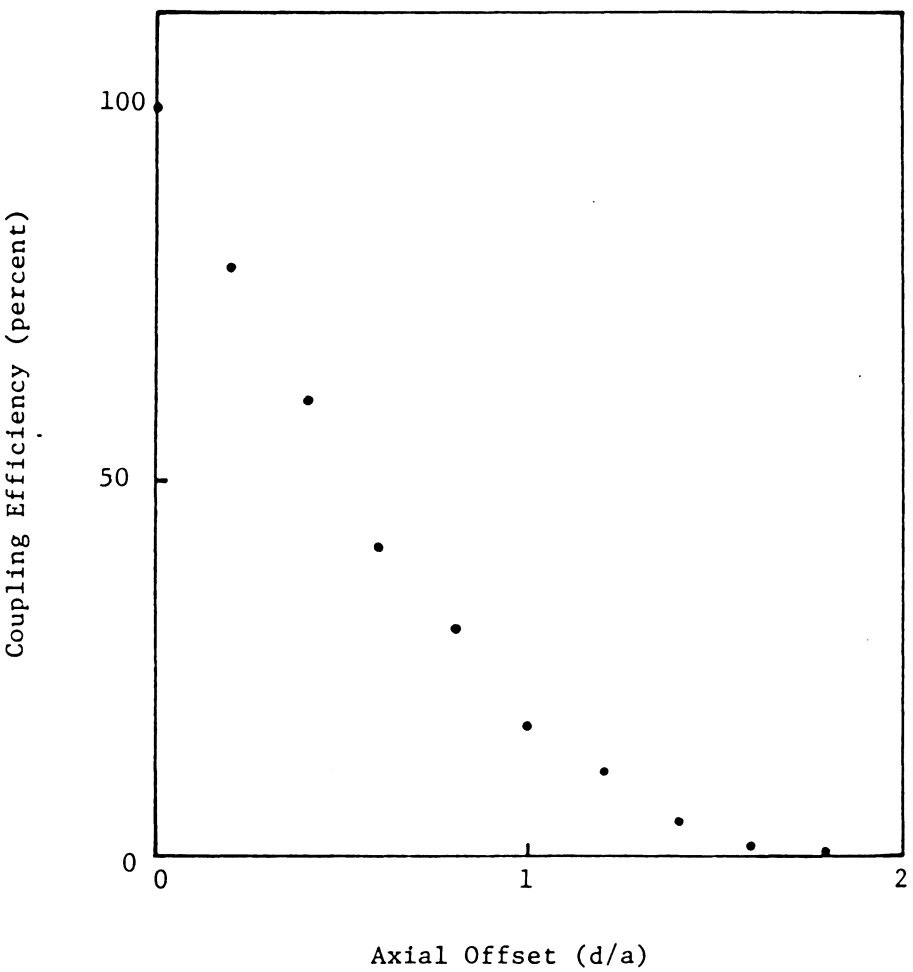

Figure 5.3.b. Coupling efficiency versus fiber axial offset; second experiment.

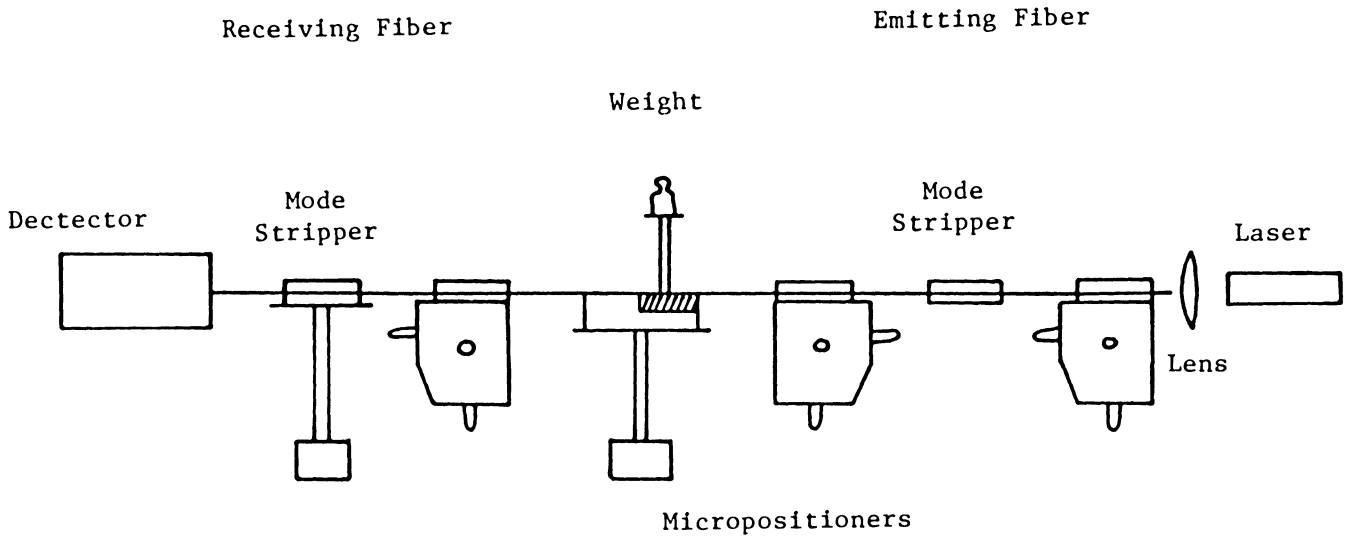

Figure 5.4. Axial offset fiber sensor.

the other half. Tapes were stuck onto the lower surface so that both halves were of the same height. Care was taken to ensure the flatness of the surface. The prepared aluminium block was then put onto an adjustable stand and just below the joint of the fiber ends.

The experiment began by aligning the fibers with the micropositioners. After optimizing the output power, the position of the aluminium block was raised by adjusting the stand such that the top surface of the block was almost attached to the fiber ends. Then epoxy was gently added onto the block. About 1.5 cm of both emitting and receiving fibers were covered by the epoxy.

The output power of the receiving fiber was decreased greatly due to the displacement of the fiber ends during the adding of epoxy. The micropositioners were immediately adjusted to obtain optimal output power before hardening of the epoxy. In the process of curing, the output power seemed to increase. This is probably because epoxy acts like a matching liquid for the fibers. Finally, the output power was stable after hardening of the epoxy. A simple construction of the axial offset fiber sensor was thus completed.

An aluminium cylindrical rod with radius of ~0.23 cm was then added onto the half of the epoxy which was cushioned by tapes. Weights were added onto a small box which was on the top of the cylinder, and the output power was recorded. Average values of four groups of data obtained were shown in Figure 5.5.

It is shown that output power decreases almost linearly with mechanical loading which is a desirable relationship. But the sensitivity of the output power to mechanical loading does not seem very good. The output power decreases 6.2 % for a weight with a mass of 0.8 kg. The sensitivity depends very much on the flexibility of the material cushioning the fiber on which a force is exerted. It is believed that the tapes are not flexible enough to allow the fiber to make a sufficient displacement when a force is exerted upon it. Additional work with more compliant backing materials are thus suggested by these preliminary results.

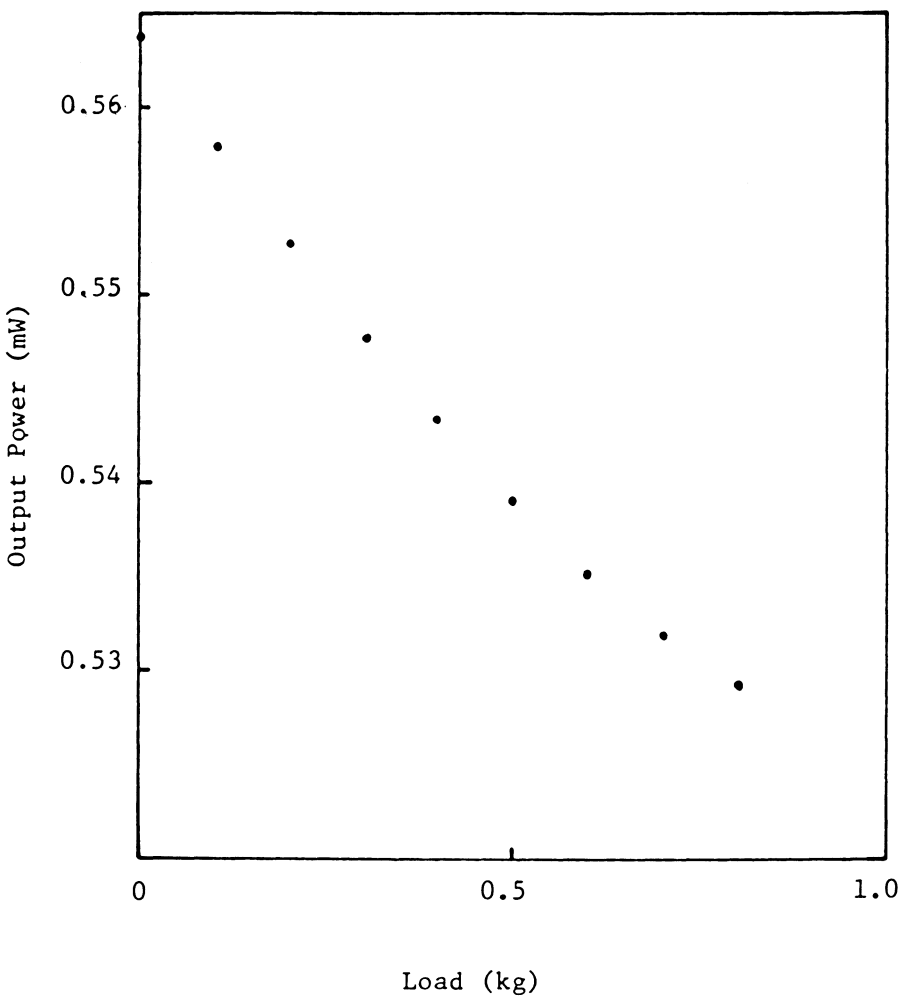

Figure 5.5. Output power versus mechanical loading.

CHAPTER VI

CONCLUSIONS AND FURTHER RESEARCH

The formulas for estimating the coupling efficiency of graded index fibers with different refractive index profiles due to axial offset were derived in this thesis. Construction of an axial offset fiber optic sensor were also described.

The coupling efficiency of the parabolic graded index fibers has been shown to be more sensitive to axial offset than the central dipped fibers. It has also been shown that the sensivity increases as α decreases. These results are obtained by assuming uniform power distribution in the fibers.

Since coupling efficiency depends strongly upon the power distribution in the fiber, the formulas obtained which based upon a uniform power distribution are not accurate enough for estimating the coupling efficiency between two long pieces of fiber. They give lower coupling efficiency values for fiber optic transmission lines (long fibers) used in communication or telemetry systems. Power distribution models for calculations of coupling efficiency between fiber

optic transmission lines are suggested by the authors of the references [12,26]. However, the assumption of a uniform power distribution is good enough for calculations of coupling efficiency between two short pieces of fiber. The contributions due to leaky modes should be included for calculations if very accurate results are required [21,27].

An approximate linear relationship between the output power and the mechanical loading has been obtained for the axial offset fiber sensor. This sensor has an advantage of simplicity which is a general characteristic of intensity-type fiber sensors. Several factors have to be considered to ensure the accuracy of this sensor. The light source used must be quite stable with temperature and environmental effects. Also, axial offset is generally accompanied by angular misalignment which is very difficult to eliminate primarily because the optical fibers are so small. This misalignment must be minimized to insure accuracy.

The constructed axial offset fiber sensor described here suffers from insufficient flexibility of the support tapes. A rubber or sponge backing might provide the needed flexibility. But the use of one of these materials might create another problem; rubber or sponge might be too spongy, so

that when a force is exerted on a fiber, an axial displacement which is more than 2a will be created. The output power in this case is practically zero. Rubber or sponge sandwiched between tapes might be the best material for providing a cushion for the fiber.Additional work is needed in this area.

The sensitivity also can be increased by several other ways. The sensitivity is increased by using fibers with smaller index profile, α . It also can be increased by using a receiving fiber with a smaller Δ than that of the emitting fiber. Theoretical results of coupling loss due to Δ mismatch and transverse offset is shown in Figure 6.1 [12]. Another way of increasing sensitivity is by using a receiving fiber with a smaller core radius than that of the emitting fiber. Four separate cases are considered by Miller to calculate coupling efficiency versus axial offset for unequal core diameters [28]. These calculations show a 33% greater sensitivity to axial offset for the parabolic profile and approximately the same sensitivity to C (the ratio of the radii) as the step profile. The results are shown in Figure 6.2. Finally, better sensitivity can be achieved by using a launch beam NA greater than or equal to the emitting fiber NA.

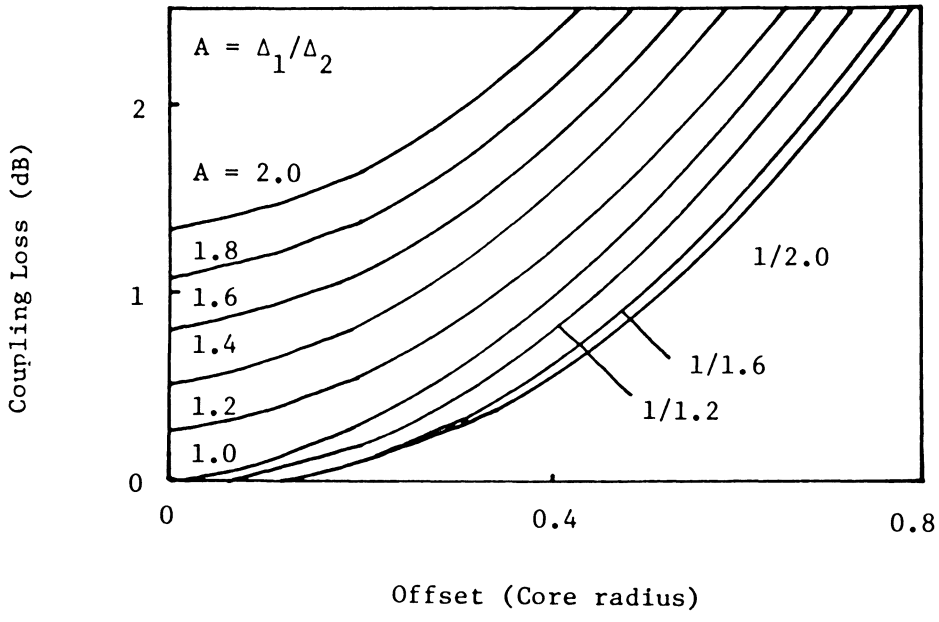

Figure 6.1. Coupling loss due to Δ mismatch and axial offset [12].

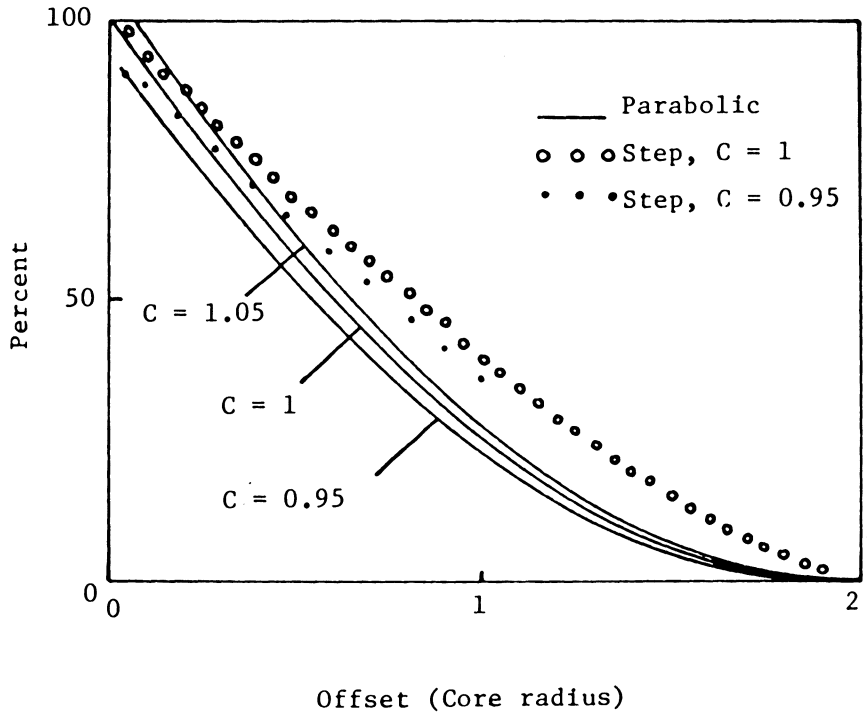

Figure 6.2. Coupling efficiency versus axial offset for unequal core diameters [19].

If sensitivity is still a problem, then both emitting and receiving fibers with a certain degree of bending might be considered for an application as a sensor. Bending loss would provide extra sensitivity for the sensor. A difficulty in constructing this sensor may be that the radius of curvature of the fibers will change if a force is exerted on the fibers. Thus, it would be very difficult to estimate the coupling efficiency.

Further research might include the construction of an axial offset fiber sensor array and imbedding this array in composite materials. Variation of the output power of the imbedded optical fibers in the composite could allow for the real time internal monitoring of composite material properties.

REFERENCES

1. K.C. Kao and G.A. Hockham, " Dielectric-fiber surface waveguides for optical frequencies, " Proc. IEE, 133 : 1151, 1966.

2. B.S. Jackson, " Optical time domain reflectometry as a nondestructive evaluation technique for composite materials, " M.S. Thesis, Virginia Tech, 1984.

3. C.M. Davis, E.F. Carome, M.H. Weik, Shaoul Ezekiel and R.E. Einzig, Fiber Optic Sensor Technology Handbook, Dynamic Systems, Inc.

4. G.B. Hocker, " Fiber optic sensing of pressure and temperature, " Applied Optics, Vol. 18, No.9, pp. 1445-1448,1979.

5. G.F. Lipscomb, S.K.Yao and C.K. Asawa, " Stabilization of single and multimode fiber optical microbend sensors, " First International Conference on Optical Fibre Sensors, p.117, 1983.

6. R.G. May, " Enhancement of multimode fiber optic microbend sensor sensitivity by refractive index profile design, " M.S. Thesis, Virginia Tech, unpublished.

7. A.H. Cherin, An Introduction to Optical Fibers, New York : McGraw- Hill, 1983.

8. Technical Staff of CSELT, Optical Fibre Communication, McGraw-Hill, 1980.

9. Dietrich Marcuse, Principles of Optical Fiber Measurement, New York : Academic Press, 1981.

10. S.D. Personick, " Receiver design for digital fiber optic communication systems, " BSTJ, Vol.52, pp. 843-874, 1973.

11. Gerd Keiser, Optical Fiber Communications, McGraw-Hill, 1983.

12. S.C. Mettler, " A general characterization of splice loss for multimode optical fibers, " BSTJ, Vol.58, No.10, P. 2163, 1979.

13. F.L. Thiel and R.M. Hawk, " Optical waveguide cable connection, " Applied Optics, Vol.15, No.11, pp.2785-2791, 1976.

14. S.Das, P.A. Goud and C.G. Englefield, " Modal analysis of loss, noise and distortion due to tilt misalignment in multimode fiber splices, " SPIE, Vol.479, pp. 104-110, 1984.

15. J.F. Dalgleish, " A review of optical fiber connection technology, " Proc. 25th Int. Wire and Cable Symp., pp. 240-246, 1976.

16. T.C. Chu and A.R. McCormick, " Measurement of loss due to offset, end separation, and angular misalignment in graded index fibers excited by an incoherent source, " BSTJ, Vol.57, No.3, pp. 595- 602, 1978.

17. R.B. Kummer, " Lightguide splice loss-effects of launch beam numerical aperture, " BSTJ, Vol.59, No.3, pp. 441-447, 1980.

18. M. Young, " Geometrical theory of multimode optical fiber-to-fiber connectors, " Optics Communications, Vol.7, No.3, pp. 253-255, 1973.

19. D. Gloge, " Offset and tilt loss in optical fiber splices, " BSTJ, Vol.55, No.7, pp. 905-916, 1976.

20. H. Tsuchiya, H. Nakagome, N. Shimizu, and S. Ohara, " Double eccentric connectors for optical fibers, " Applied Optics, Vol.16, No.5, pp. 1323-1331, 1977.

21. P. Di Vita and U. Rossi, " Theory of power coupling between multimode optical fibers, " Optical and Quantum Electronics, Vol.10, pp. 107-117, 1978.

22. P. Di Vita and R. Vannucci, " Geometrical theory of coupling errors in dielectric optical waveguides, " Optics Communications, Vol.14, No.1, pp. 139-144, 1975.

23. A. H. Cherin and P.J. Rich, " Measurement of loss and output numerical aperture of optical fiber splices, " Applied Optics, Vol.17, No.4, pp. 642-645, 1978.

24. Matsumoto and K. Nakagawa, " Wavelength dependence of spliced graded-index multimode fibers, " Applied Optics, Vol.18, No.9, pp. 1449-1454, 1979.

25. P. Di Vita and U. Rossi, " Evaluation of splice losses induced by mismatch in fibre parameters, " optical and Quantum Electronics, Vol.13, pp. 91-94, 1981.

26. C.M. Miller and S.C. Mettler, " A loss modal for parabolic-profile fiber splices, " BSTJ, Vol.57, No.9, pp. 3167-3180, 1978.

27. R. Olshansky, " Leaky modes in graded index optical fibers, " Applied Optics, Vol.15, No.11, pp. 2773-2777, 1976.

28. C.M. Miller, " Transmission versus transverse offset for parabolic- profile fiber splices with unequal core diameters, " BSTJ, Vol.55, No.7, pp. 917-926, 1976.

The vita has been removed
from the scanned document